Polarization of protease-activated receptor 2 (PAR-2) signaling is altered during airway epithelial remodeling and deciliation

Received for publication, January 17, 2020, and in revised form, March 31, 2020 Published, Papers in Press, April 2, 2020, DOI 10.1074/jbc.RA120.012710

Ryan M. Carey[‡], Jenna R. Freund[‡], Benjamin M. Hariri[‡], Nithin D. Adappa[‡], James N. Palmer[‡], and Robert J. Lee[‡§1]

From the Departments of [‡]Otorhinolaryngology–Head and Neck Surgery and [§]Physiology, University of Pennsylvania Perelman School of Medicine, Philadelphia, Pennsylvania 19104

Edited by Mike Shipston

Protease-activated receptor 2 (PAR-2) is activated by secreted proteases from immune cells or fungi. PAR-2 is normally expressed basolaterally in differentiated nasal ciliated cells. We hypothesized that epithelial remodeling during diseases characterized by cilial loss and squamous metaplasia may alter PAR-2 polarization. Here, using a fluorescent arrestin assay, we confirmed that the common fungal airway pathogen *Aspergillus fumigatus* activates heterologously-expressed PAR-2. Endogenous PAR-2 activation in submerged airway RPMI 2650 or NCI–H520 squamous cells increased intracellular calcium levels and granulocyte macrophage–colony-stimulating factor, tumor necrosis factor α, and interleukin (IL)-6 secretion. RPMI 2650 cells cultured at an air–liquid interface (ALI) responded to apically or basolaterally applied PAR-2 agonists. However, well-differentiated primary nasal epithelial ALIs responded only to basolateral PAR-2 stimulation, indicated by calcium elevation, increased cilia beat frequency, and increased fluid and cytokine secretion. We exposed primary cells to disease-related modifiers that alter epithelial morphology, including IL-13, cigarette smoke condensate, and retinoic acid deficiency, at concentrations and times that altered epithelial morphology without causing breakdown of the epithelial barrier to model early disease states. These altered primary cultures responded to both apical and basolateral PAR-2 stimulation. Imaging nasal polyps and control middle turbinate explants, we found that nasal polyps, but not turbinates, exhibit apical calcium responses to PAR-2 stimulation. However, isolated ciliated cells from both polyps and turbinates maintained basolateral PAR-2 polarization, suggesting that the calcium responses originated from nonciliated cells. Altered PAR-2 polarization in disease-remodeled epithelia may enhance apical responses and increase sensitivity to inhaled proteases.

Protease-activated receptors (PARs)[2] are G-protein–coupled receptors (GPCRs) that can drive inflammation in asthma, chronic rhinosinusitis (CRS), and allergic rhinitis (1, 2). PARs are activated by proteolytic cleavage of the extracellular N terminus, exposing an intramolecular tethered ligand (1, 2). PAR-2 may be activated by mast cell tryptase (3), neutrophil elastase (4), *Alternaria* fungal proteases (5), and house dust mite proteases (6) to promote T helper 2 (Th_2) inflammation in bronchial epithelial cells (7). We previously found that PAR-2 is expressed on the basolateral membrane of healthy and well-polarized differentiated primary sinonasal epithelial ciliated cells, where it elevates intracellular calcium to increase ciliary beating and apical membrane Cl^- secretion (8), suggesting PAR-2 promotes epithelial mucociliary clearance in response to protease activity.

We hypothesized basolateral polarization of PAR-2 may limit its activation except during times of epithelial barrier breakdown during infection or inflammation. Alteration of epithelial polarization or cell-type composition occurs in obstructive airway diseases such as asthma and COPD (9, 10). Loss of airway cilia may occur with viral or bacterial infection (11–14), type-2 inflammation-driven remodeling (15), or smoking (16, 17). Squamous metaplasia occurs after bacterial infection, particularly in cystic fibrosis-related CRS (18), and is frequently reported in tissue samples from CRS patients (19, 20).

Much of the literature on airway remodeling focuses on barrier dysfunction, but airway cells *in vitro* can maintain tight

This work was supported in part by National Institutes of Health Grants R01DC016309 and R21AI137484 and Cystic Fibrosis Foundation Grant LEE19G0 (to R. J. L.). The authors declare that they have no conflicts of interest with the contents of this article. The content is solely the responsibility of the authors and does not necessarily represent the official views of the National Institutes of Health.

This article contains Figs. S1–S9, Table S1, and supporting Refs. 1–38.

[1] To whom correspondence should be addressed: Dept. of Otorhinolaryngology–Head and Neck Surgery, Hospital of the University of Pennsylvania, Ravdin Bldg., 5th Fl., Ste. A, 3400 Spruce St., Philadelphia, PA 19104. Tel.: 215-573-9766; E-mail: rjl@pennmedicine.upenn.edu.

[2] The abbreviations used are: PAR, protease-activated receptor; PAR-2, protease-activated receptor 2; ALI, air–liquid interface; ASL, airway–surface liquid; β2AR, β2 adrenergic receptor; CaCC, calcium-activated chloride channel; CBF, ciliary beat frequency; CBX, carbenoxolone; CCh, carbachol; CF, cystic fibrosis, CFTR, cystic fibrosis transmembrane conductance regulator; CM, conditioned media; COPD, chronic obstructive pulmonary disease; CRS, chronic rhinosinusitis; CSC, cigarette smoke condensate; ELISA, enzyme-linked immunosubstrate assay; FITC, fluorescein isothiocyanate; 2FLI, 2-furoyl-LIGRLO-NH_2, PAR-2 agonist; GM-CSF, granulocyte macrophage–colony-stimulating factor; GPCR, G-protein–coupled receptor; HBSS, Hanks' balanced salt solution; IF, immunofluorescence; IL-13, interleukin 13; LDH, lactate dehydrogenase; MEM, minimal essential medium; NKCC1, $Na^+K^+2Cl^-$ cotransporter; PFC, perfluorocarbon; PTX, pertussis toxin; R.A., retinoic acid; TEER, transepithelial electrical resistance; TG-1, transglutaminase 1; TGF-β2, transforming growth factor β2; DMEM, Dulbecco's modified Eagle's medium; ANOVA, analysis of variance; qPCR, quantitative PCR; BEBM, bronchial epithelial basal medium; AM, acetoxymethyl ester; $[Ca^{2+}]_i$, intracellular calcium concentration; TRITC, tetramethylrhodamine isothiocyanate; BAPTA, 1,2-bis(2-aminophenoxy)ethane-*N,N,N′,N′*-tetraacetic acid; Th_2, T helper 2.

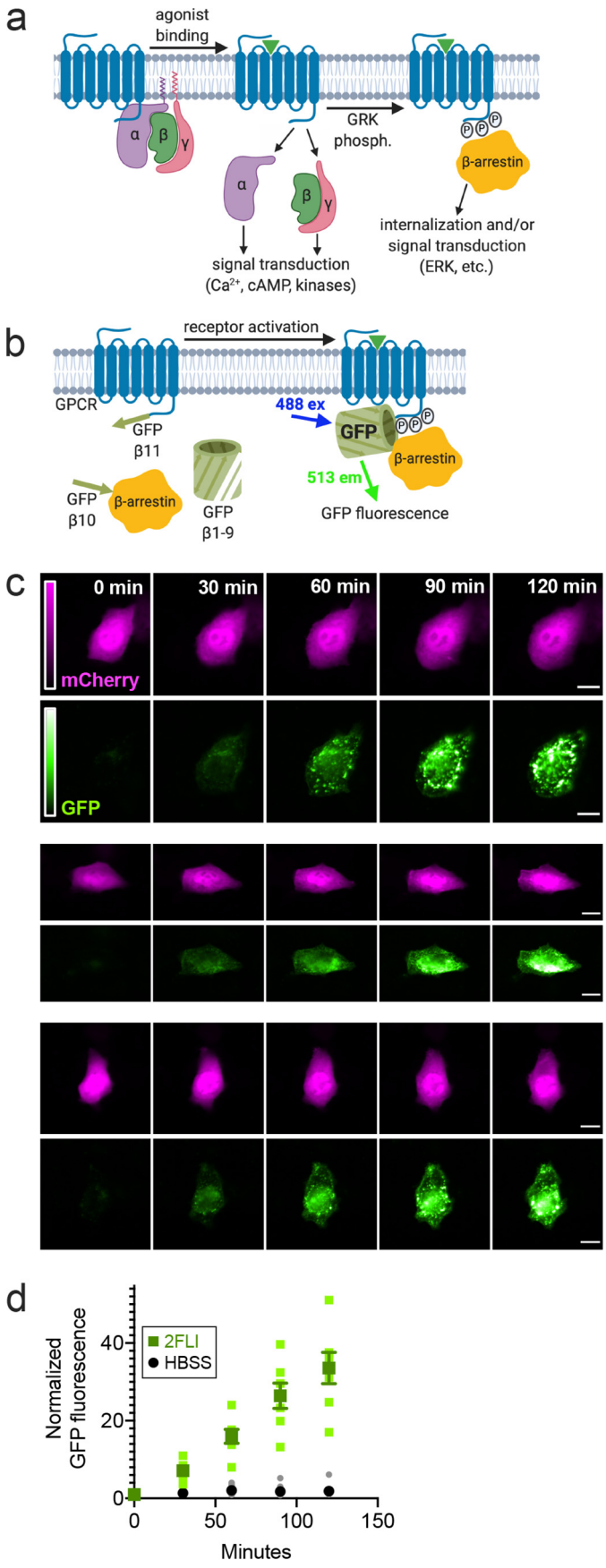

Figure 1. *A. fumigatus* CM directly activates PAR-2 in airway cells. *a,* diagram of GPCR interaction with β-arrestin after activation and phosphorylation by G-receptor kinase (*GRK*) *b,* diagram of the Trio assay (modified from Ref. 26) used to detect PAR-2 activation. A heterologously-expressed GPCR (in this case PAR-2) is tagged at the C-terminal end with the β11-strand of GFP. The receptor is co-expressed with β-arrestin tagged with the β10-strand of GFP along with soluble GFP β-strands 1–9. Association of the PAR-2 with β-arrestin allows the formation of a complete fluorescent GFP molecule; soluble mCherry is included on the plasmid as a transfection control (not shown in the model). *c,* representative images of A549 cells expressing PAR-2 Trio components (plus mCherry as transfection control) stimulated with 10 μM 2FLI for 0–120 min. *Scale bars* are 15 μm. *d,* normalized GFP fluorescence in cells stimulated with 2FLI or buffer alone (HBSS) at time points taken over 2 h. Data points are independent experiments imaged on three different days ($n = 5–9$). *a* and *b* were created with Biorender.com.

junctions and barrier function despite substantial morphological changes, including loss of cilia (12). Less is known about how signaling is altered before large-scale barrier breakdown in severe disease. We hypothesized that loss of epithelial polarization may affect PAR-2 signaling independently of barrier disruption, perhaps sensitizing cells to protease allergens.

We first tested activation of PAR-2 by *Aspergillus fumigatus,* the most prevalent fungal cause of pulmonary allergic disease, including allergic bronchopulmonary aspergillosis associated with chronic lung injury in patients with cystic fibrosis (CF) or chronic asthma (21). We next examined PAR-2 signaling in airway squamous cells using pharmacology and live-cell imaging. We then tested PAR-2 signaling in well-differentiated air–liquid interface (ALI) cultures of primary nasal cells exposed to disease-related modifiers, including IL-13, CSC, and retinoic acid deficiency, all of which alter epithelial morphology. We also examined isolated tissue from inflamed nasal polyp and compared it with control middle turbinate. The data below reveal important alterations of the polarity of PAR-2 signaling in squamous cells and primary epithelial cells de-differentiated through disease-relevant mechanisms.

Results

A. fumigatus conditioned media can directly activate PAR-2

Although *Alternaria* proteases are well-documented to activate PAR-2 (22, 23), evidence exists that *A. fumigatus* also activates PAR-2 in the airway (7) and cornea (24). *A. fumigatus* is a common cause of allergic bronchopulmonary aspergillosis or allergic fungal rhinosinusitis (21) and can cause fatal invasive aspergillosis (25). We sought to first confirm whether *A. fumigatus* produces PAR-2–activating proteases, as this is highly important for considering the role of PAR-2 in aspergillosis and fungal sinusitis.

We utilized a fluorogenic assay (Trio assay) to directly visualize PAR-2 activation by its interaction with β-arrestin (26), which associates with activated and phosphorylated GPCRs and mediates further signal transduction and/or internalization to endosomes (Fig. 1*a*) (27). This assay is based on a tripartite GFP, with the 11th β-strand of GFP fused to the C terminus of PAR-2, the 10th β-strand of GFP fused to β-arrestin, and β-strands 1–9 of GFP expressed as a soluble protein (26). When PAR-2 is activated, association of PAR-2 with β-arrestin allows a complete GFP to form and increases fluorescence (Fig. 1*b*). This approach eliminates other effects that may impinge on downstream signaling (*e.g.* toll-like receptor activation during exposure to fungus-conditioned media) by allowing us to look

directly at the binding of arrestin to the receptor after receptor activation. We visualized PAR-2 activation via appearance of GFP fluorescence in A549 alveolar-like cells (Fig. 1*c*). Stimulation with PAR-2 peptide agonist 2FLI resulted in the appearance of punctate GFP fluorescence over the course of 2 h (Fig. 1, *c* and *d*).

In cells imaged at 90 min, 2FLI increased GFP fluorescence ~30-fold, whereas PAR-4 agonist AY-NH_2 had no effect (Fig. 2*a*). Two other PAR-2 agonists (AC 55541 and SLIGRL-NH_2) similarly increased GFP fluorescence, whereas scrambled LRGILS-NH_2, cholinergic agonist carbachol (CCh), histamine, or purinergic receptor agonist ATP had no effect on PAR-2 activation (Fig. 2*b*). Exposure to conditioned media (CM) from *A. fumigatus*, but not *Aspergillus niger*, increased GFP fluorescence (Fig. 2*c*), signaling PAR-2 activation. Heat inactivation of the CM (100 °C for 20 min) eliminated PAR-2 activation (Fig. 2*c*). No activation of the β2 adrenergic receptor (β2AR) with fungus-conditioned media was observed, although β2AR activation was observed with isoproterenol (Fig. 2*d*). These results support that *A. fumigatus* activates PAR-2, likely via a secreted heat-labile protease.

Similarly, in PAR-2 Trio-transfected BEAS-2B immortalized bronchial cells, we also observed activation of GFP fluorescence by 2FLI but not AY-NH_2 (Fig. 3, *a–f*), supporting results observed in A549 cells. We likewise observed PAR-2 activation by *A. fumigatus* but not *A. niger* in BEAS-2B cells (Fig. 3, *g–k*).

Controversy exists over whether certain host and pathogen proteases activate PAR-2 by cleavage at the activating site or inhibit PAR-2 by cleavage downstream, removing the tethered ligand and "disarming" it (28). Neutrophil and *Pseudomonas aeruginosa* elastase have both been suggested to either activate (4, 29, 30) or disarm PAR-2 (31, 32). Differential results may be due to altered protein processing in different cell types or the different assays used. We tested whether several proteases implicated in allergy can activate PAR-2 expressed in airway cells using this assay. We observed PAR-2 activation with human lung tryptase, neutrophil elastase, and dust mite protease Der p 3 in BEAS-2B cells (Fig. 3, *l–r*). Together, these data verify activation of PAR-2 by *A. fumigatus* as well as common lung proteases.

To test whether *A. fumigatus* activates PAR-2 G-protein signaling as well as arrestin binding, we imaged A549s loaded with the calcium indicator Calbryte 590. A red calcium indicator was used to reduce effects of autofluorescence of the fungal media during acute addition. We and others previously showed that PAR-2 is linked to calcium in airway epithelial cells (8). It is important to note that arrestin binding and G-protein signaling are not mutually exclusive, and our goal was not to quantify the relative contributions of these two pathways (*e.g.* agonist biasing) in this study. Although the Trio assay above allowed examination of heterologous PAR-2 directly (via arrestin binding), measuring calcium responses as a readout of GPCR-driven G-protein signaling allows examination of signaling of endogenous PAR-2.

Stimulation of untransfected A549s with dilute (25%) *A. fumigatus* media activated a calcium response that was reduced ~50% by incubation with PAR-2 antagonists FSLLRY-NH_2 or AZ3451 or by heat treatment (Fig. 4, *a* and *b*). This is likely because *A. fumigatus* media contain multiple secreted products and metabolites that can impinge on calcium, including proteases that appear to activate PAR-2. When *A. fumigatus* CM was dialyzed overnight against HBSS to remove small molecules and equilibrate salts but to retain larger proteins (6–8 MWCO dialysis tubing), we observed calcium signals that were more completely inhibited by FSLLRY-NH_2 or heat treatment (Fig. 4, *c* and *d*). These results confirm activation of PAR-2 by *A. fumigatus* (7, 24) and support a potential role for this protein in the airway response to fungal pathogens beyond *Alternaria*. We next sought to examine how PAR-2 signaling might change in airway squamous cells, as squamous epithelial de-differentiation is commonly observed in airway diseases, as described above.

PAR-2 is expressed and functional in squamous airway epithelial cells

We observed expression of PAR-2 in nasal septal squamous RPMI 2650 cells (Fig. S1). PAR-2 peptide agonist 2FLI or activating protease trypsin increased intracellular calcium (Fig. S2). PAR-4 agonist peptide AY-NH_2 or activating protease thrombin had no effect (Fig. S2). PAR-2 activation also transiently activated protein kinase C (Fig. S3) in both RPMI 2650 and lung squamous cell line NCI–H520.

We also observed activation of PAR-2 by human lung tryptase and Der p 3 (Fig. S4). PAR-2 activation also had a small but significant effect of acutely-reducing squamous cell line metabolism and/or proliferation through lowering of cAMP, but did not activate apoptosis (Fig. S5). PAR-2 activation increased secretion of TNFα and GM-CSF from RPMI 2650 cells and IL-6 and GM-CSF from NCI–H520 cells, likely involving dual coupling to G_q and G_i G-protein isoforms (Fig. S6). Thus, PAR-2 in airway squamous cells may regulate inflammation. To understand whether this is reflective of squamous phenotype or the tumor origin of these cells, we next tested how PAR-2 signaling and polarization change with epithelial de-differentiation and/or remodeling using primary cells.

Primary airway epithelially-ciliated ALI cultures can be dedifferentiated/remodeled by exposure to a type 2 cytokine or submersion

To begin to understand how epithelial remodeling changes polarization of PAR-2 in primary sinonasal cells, we initially de-differentiated/remodeled primary ciliated ALI cultures by two methods. The first was exposure to IL-13 (10 ng/ml, basolateral), which induces cilia loss and goblet cell metaplasia (33, 34). The second was apical submersion, which induces a more squamous phenotype (33, 35). ALIs were cultured for 21 days to establish a well-ciliated baseline (Fig. 5*a*). IL-13 or apical submersion both resulted in a decrease in the number of ciliated cells over 6 days, shown by a reduction in β-tubulin IV immunofluorescence (Fig. 5, *a* and *b*). Although IL-13 increased goblet cell-specific Muc5AC intensity (Fig. 5, *a* and *c*), submersion only minimally increased Muc5AC at 6 days (Fig. 5, *a* and *c*). Submersion instead increased expression of transglutaminase 1 (TG-1; measured via ELISA), previously reported to reflect squamous differentiation (Fig. 5*d*) (36, 37). Transepithelial electrical resistance (TEER) remained intact up to 4 days (Fig. 5*e*), and maintenance of epithelial barrier function was confirmed by measurement of FITC-conjugated dextran flux at day 4 as well as ability of cells to maintain low apical glucose levels

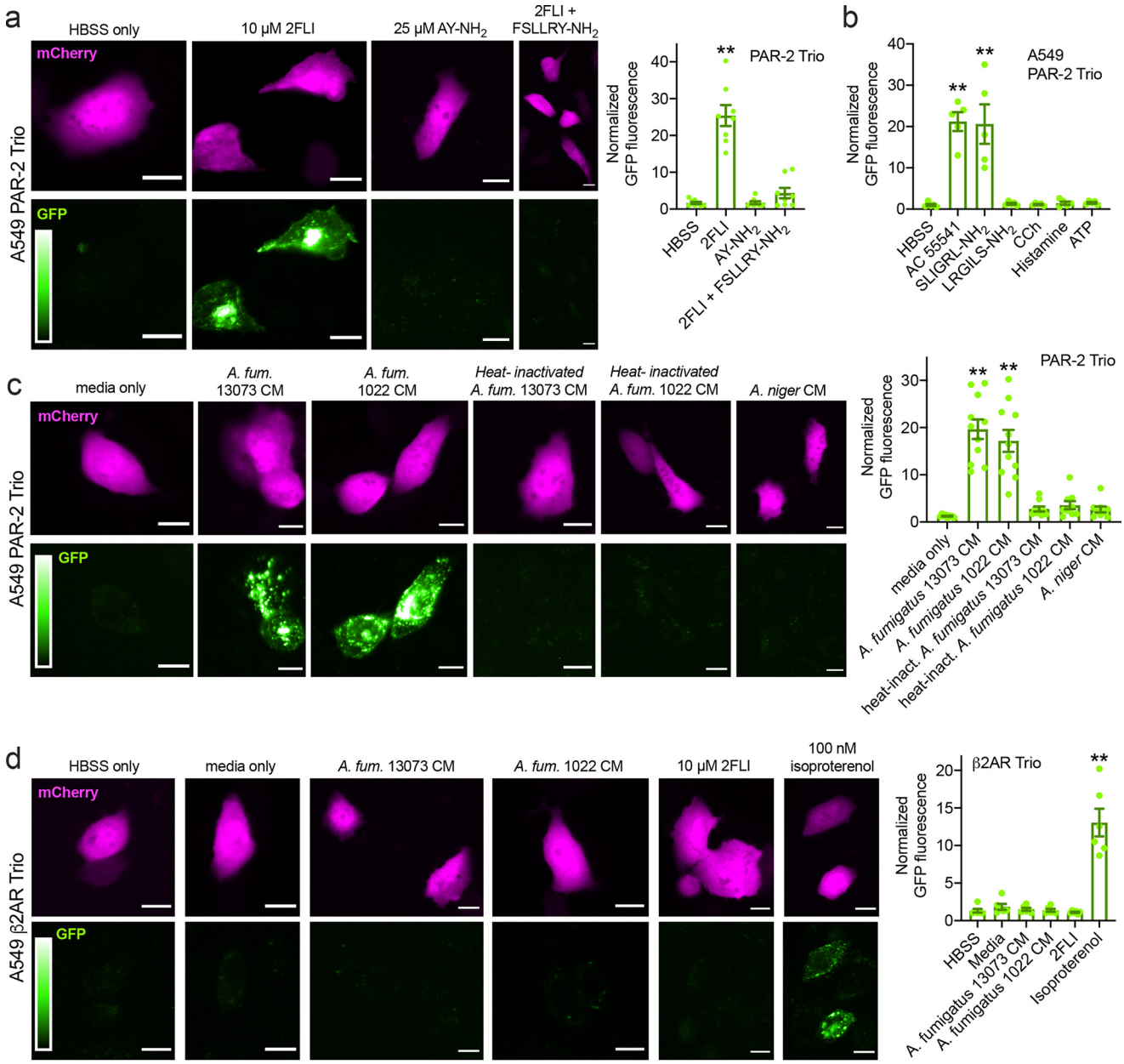

Figure 2. Activation of PAR-2 by peptide PAR-2 agonist and *A. fumigatus* CM in A549 cells. Cells were transfected with the PAR-2 Trio system (26) as described in the text to detect receptor–β-arrestin interaction upon PAR-2 activation. Many other studies have already demonstrated that β-arrestin is recruited to PAR-2 upon activation (26, 29, 30, 74–78). Using this assay allows us to directly look at PAR-2 activation in the absence of any other signals downstream of other targets of proteases and/or CM that could impinge on the PAR-2 signaling pathway. *a*, after 90 min stimulation with PAR-2 agonist 2FLI, GFP fluorescence was increased ~25-fold compared with buffer (HBSS) only or PAR-4–activating peptide AY-NH_2. The GFP fluorescence increase, signaling PAR-2 activation, was lost when cells were stimulated with 2FLI in the presence of 10 μM PAR-2 antagonist FSLLRY-NH_2. *b*, *bar graph* showing data from experiments as in *a* with alternative PAR-2 agonists AC 55541 and SLIGRL-NH_2 plus scrambled LRGILS-NH_2 and cholinergic agonist CCh, histamine, and purinergic agonist ATP (100 μM each). *c*, representative images of PAR-2 activation with *A. fumigatus* (*A. fum.*) CM. Cells were exposed to conditioned media for 10 min followed by washing and resuspension in HBSS for 90 min. *Bar graph on right* shows normalized GFP fluorescence. Significance was determined by one-way ANOVA with Dunnett's post-test comparing values to media only control; **, $p < 0.01$. *d*, A549 cells were transfected with β2AR Trio. *A. fumigatus* CM did not activate β2AR but 100 nM isoproterenol did. *Bar graph* shows quantification of results. *All bars* show data points from ≥7 independent experiments imaging fields from independent transfected wells on separate days. Significance was determined by one-way ANOVA with Dunnett's post-test comparing all values to HBSS alone; **, $p < 0.01$. *Scale bars* are 15 μm.

(Fig. S7*a*). Evidence of cell death (LDH release) was not observed (Fig. S7*b*).

We thus chose the 4-day exposure time to IL-13 or submersion (21 days of differentiation plus a further 4 days of IL-13 or submersion, here termed Day 21 + 4) for further experiments as it was a time point when the epithelium was remodeled but barrier function remained intact. At this time point, we saw no differences in expression of PAR-2 by qPCR (Fig. S7*c*), which mimicked a lack of differences observed in nasal polyp tissue (frequently characterized by type 2 inflammation) and control middle turbinate tissue (Fig. S7*c*), in contrast to another study (38). As a control, we did see increased expression of PAR-2 in ALIs after stimulation with lipopolysaccharide, agreeing with previous results from bronchial fibroblasts (Fig. S7*c*) (39).

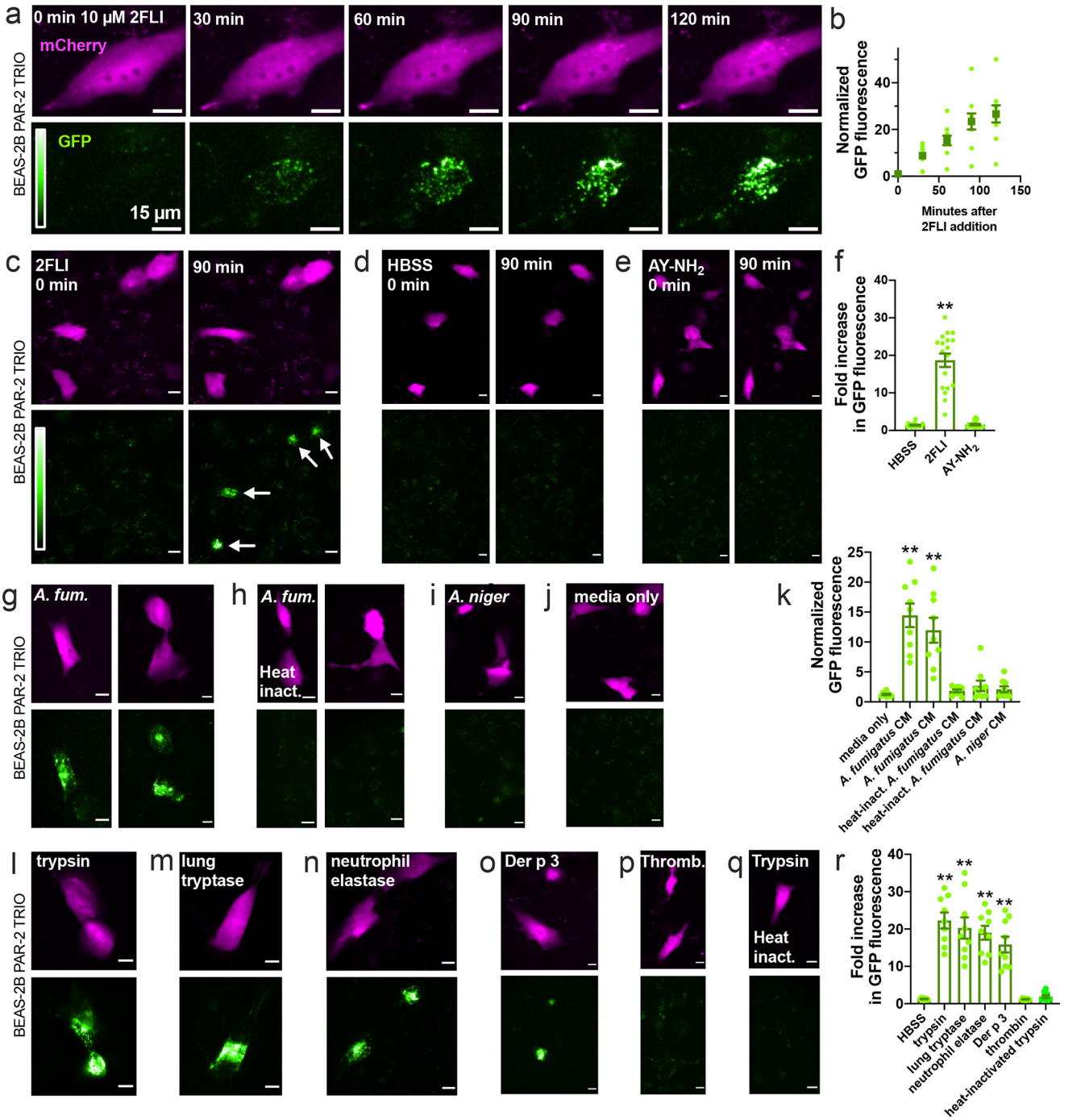

Figure 3. *A. fumigatus* CM and immune cell proteases activate PAR-2 in BEAS-2B immortalized squamous bronchial epithelial cells. *a* and *b*, representative images (*a*) and quantification (*b*) showing time course of PAR-2–arrestin recruitment and the resulting increase in GFP fluorescence in BEAS-2B cells transfected with the PAR-2 Trio assay components and stimulated with PAR-2 agonist 2FLI (26). *c–f*, after 90 min stimulation, 2FLI (*c*) but not HBSS alone (*d*) or AY-NH_2 (*e*) resulted in ~20-fold increased GFP fluorescence, quantified in *f*. *g–k*, cells were stimulated for 10 min with 25% *A. fumigatus* (*A. fum.*) CM (*g*, strain 13073 *left* and 1022 *right*), heat-inactivated *A. fumigatus* CM (*h*; 20 min; 100 °C; strain 13073 *left* and 1022 *right*), *A. niger* CM (*i*), or media only (*j*) diluted in HBSS, followed by washing with HBSS and incubation for 90 min. GFP quantification is shown in *k*. *l–r*, cells were stimulated for 10 min with 25 nM trypsin (*l*), human lung tryptase (*m*), neutrophil elastase (*n*), Der p 3 (*o*), thrombin (*p*), or heat-inactivated trypsin (*q*), followed by washing with HBSS and incubation for 90 min. Quantification of GFP fluorescence is shown in *r*. Data points in *b*, *f*, *k*, and *f* are independent experiments performed on different days ($n \geq 5$). Significance was determined by one-way ANOVA with Dunnett's post-test comparing all values to HBSS alone; **, $p < 0.01$. *Scale bars* are 15 μm.

Epithelial remodeling is associated with altered polarization of PAR-2 signaling

In primary ALIs at 5 days after seeding, when ALIs have electrical resistance but cilia have not yet developed, both apical or basolateral 2FLI or trypsin induced calcium responses (Fig. 6, *a* and *f*). After a saturating dose of apical 2FLI, another increase in apical 2FLI did not elicit a further response, whereas application of basolateral 2FLI did (Fig. 6*a*, *left*). This suggests that two separate pools of PAR-2 receptors exist, separated by the apical-to-basolateral tight-junction diffusion barrier. By day 21, responses to apical 2FLI or trypsin were lost, whereas responses to basolateral stimulation were intact (Fig. 6, *b* and *f*).

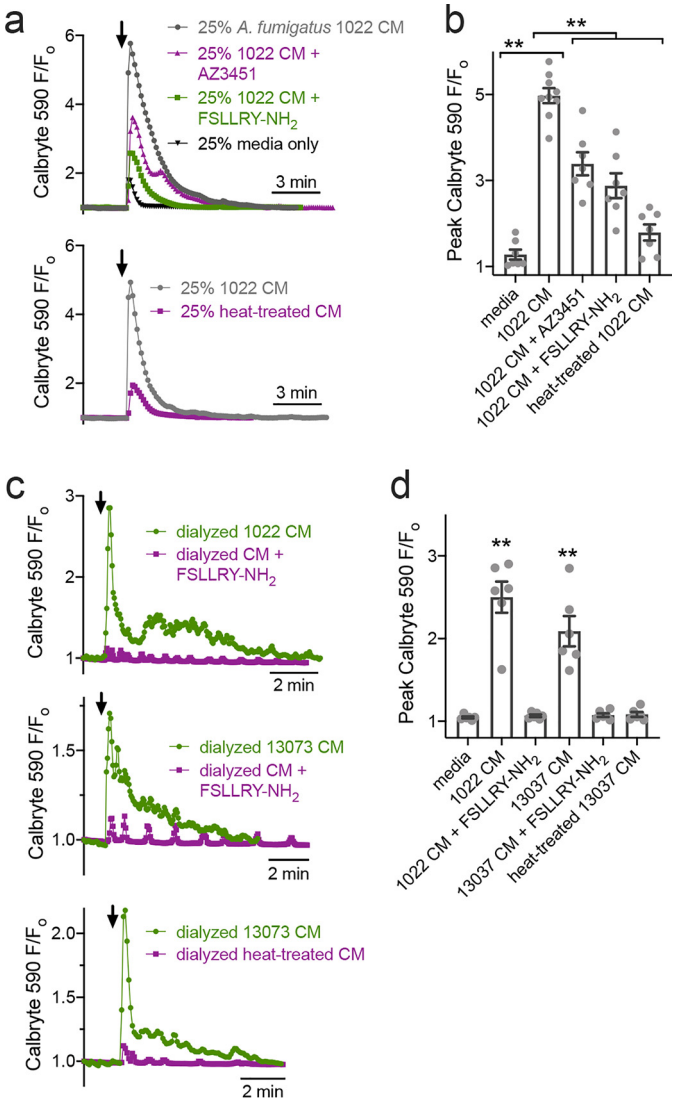

Figure 4. *A. fumigatus* CM activates PAR-2–dependent calcium responses in A549 airway cells. *a*, representative calcium traces in response to *A. fumigatus* CM (strain 1022) diluted 1:4 in HBSS (*gray*). Also shown are responses to media only (*black*), CM + 100 μM FSLLRY-NH_2 (*green*), CM + 100 μM AZ3451 (*pink, top graph*), or CM after heat treatment (100 °C for 20 min; *pink, bottom graph*). *b*, peak responses from independent experiments (n = 6–8) as shown in *a*. Significance was determined by one-way ANOVA with Bonferroni post-test; **, $p < 0.01$. *c*, representative calcium traces in response to dialyzed *A. fumigatus* CM (strain 1022 or 13073 as indicated) shown in *green*. Also shown are responses to dialyzed CM in the presence of FSLLRY-NH_2 (*pink, top* and *middle graphs*) or CM after heat treatment (*pink, bottom graph*). *d*, peak responses from independent experiments (n = 6–8) as shown in *c*. Significance was determined by one-way ANOVA with Dunnett's post-test comparing all values to dialyzed media alone; **, $p < 0.01$.

If primary cells were incubated for a further 4 days with the apical side submerged (Day 21 + 4 submerged) to promote squamous de-differentiation, the response to apical 2FLI was again observed (Fig. 6, *c* and *f*). Basolateral application of antagonist FSLLRY-NH_2 blocked the response to basolateral but not apical 2FLI (Fig. 6*c*, *right*), ruling out 2FLI diffusion across the epithelial barrier to the basolateral side. Similar results were seen at ALIs after four subsequent days of basolateral IL-13 (Fig. 6*d*). If primary ALIs were carried out to day 25 with no IL-13 and no apical submersion, only basolateral 2FLI responses were observed (Fig. 6*f*). RPMI 2650 squamous cells cultured at ALI also had 2FLI responses with application to either the basolateral or apical side; basolateral addition of antagonist blocked basolateral but not apical responses (Fig. 6, *e* and *f*). No significant differences in TEERs were observed (Fig. 6*g*).

Altered PAR-2 polarization increases epithelial fluid secretion during apical exposure to a PAR-2 agonist

We measured airway–surface liquid (ASL) height in primary ALIs. Physiological ASL was labeled with Texas Red dextran sonicated in perfluorocarbon (PFC), and ASL height was measured from orthogonal confocal slices. Primary ALIs were compared at differentiation day 25 (Fig. 7*a*) or after 21 days + 4 subsequent days IL-13 (Fig. 7*b*). Baseline ASL height was not different. Basolateral 2FLI caused an increase in ASL height in both groups (Fig. 7, *a–c*) that was inhibited by basolateral application of the $Na^+K^+2Cl^-$ co-transporter inhibitor bumetanide (Fig. 7*c*), showing that this reflected fluid secretion. However, when 2FLI was added to the apical side in PFC, IL-13–treated cultures, but not control cultures, exhibited increased ASL height (Fig. 7, *a–c*) that was blocked by calcium-activated Cl^- channel (CaCC) inhibitor $CaCC_{inh}$–A01 but not $CFTR_{inh}$–172 (Fig. 7, *b* and *c*).

Similar responses to apical 2FLI were observed after 21 days of differentiation + 4 days of submersion (Fig. 7*c*). We performed experiments using cells from CF patients homozygous for ΔF508 CFTR. CF ALIs robustly secreted fluid in response to PAR-2 stimulation (Fig. 7*d*). The responses to 2FLI were inhibited by the PAR-2 antagonist FSLLRY-NH_2 (Fig. 7*e*), confirming they were indeed due to PAR-2. These data suggest that apical PAR-2 agonist exposure does not result in epithelial fluid secretion in well-differentiated cultures, but remodeling or dedifferentiation results in apical PAR-2–activated fluid secretion via CaCC.

Epithelial remodeling and altered PAR-2 polarization enhances cytokine secretion during apical exposure to PAR-2 agonists

To further examine the effects of PAR-2 signaling alterations above, we examined secretion of TGF-β2, an important epithelium-derived cytokine in type 2 airway diseases (40). In RPMI 2650 ALIs, TGF-β2 secretion was activated by basolateral 2FLI and inhibited ~50% by the G_i inhibitor pertussis toxin (PTX; Fig. 8*a*). In contrast, activation of the TNFα receptor, which is not a GPCR, increased TGF-β2 that was not inhibited by PTX (Fig. 8*a*). In primary differentiated ALIs, apical 2FLI had no effect, but basolateral 2FLI increased TGF-β2 that was inhibited by basolateral but not apical FSLLRY-NH_2 (Fig. 8*b*). Similarly, apical trypsin or lung tryptase had little effect, whereas basolateral trypsin and tryptase increased TGF-β2 secretion (Fig. 8*b*).

In RPMI 2650 ALIs or ALIs exposed to 4 days of submersion, apical 2FLI increased TGF-β2 (Fig. 8*c*). It also potentiated TGF-β2 secretion in the presence of TNFα (Fig. 8*c*). In RPMI 2650 ALIs and primary ALIs treated with basolateral TNFα, basolateral 2FLI caused a further increase of TGF-β2 beyond TNFα alone (Fig. 8*c*). In RPMI 2650s and ALIs exposed to 4 days of submersion, this occurred with apical 2FLI as well (Fig. 8*c*). Similar results were observed in mouse nasal septum ALI cultures, with responses lost in ALIs from PAR-2 knockout (par-$2^{-/-}$) mice (Fig. S8). Further confirming the specificity of

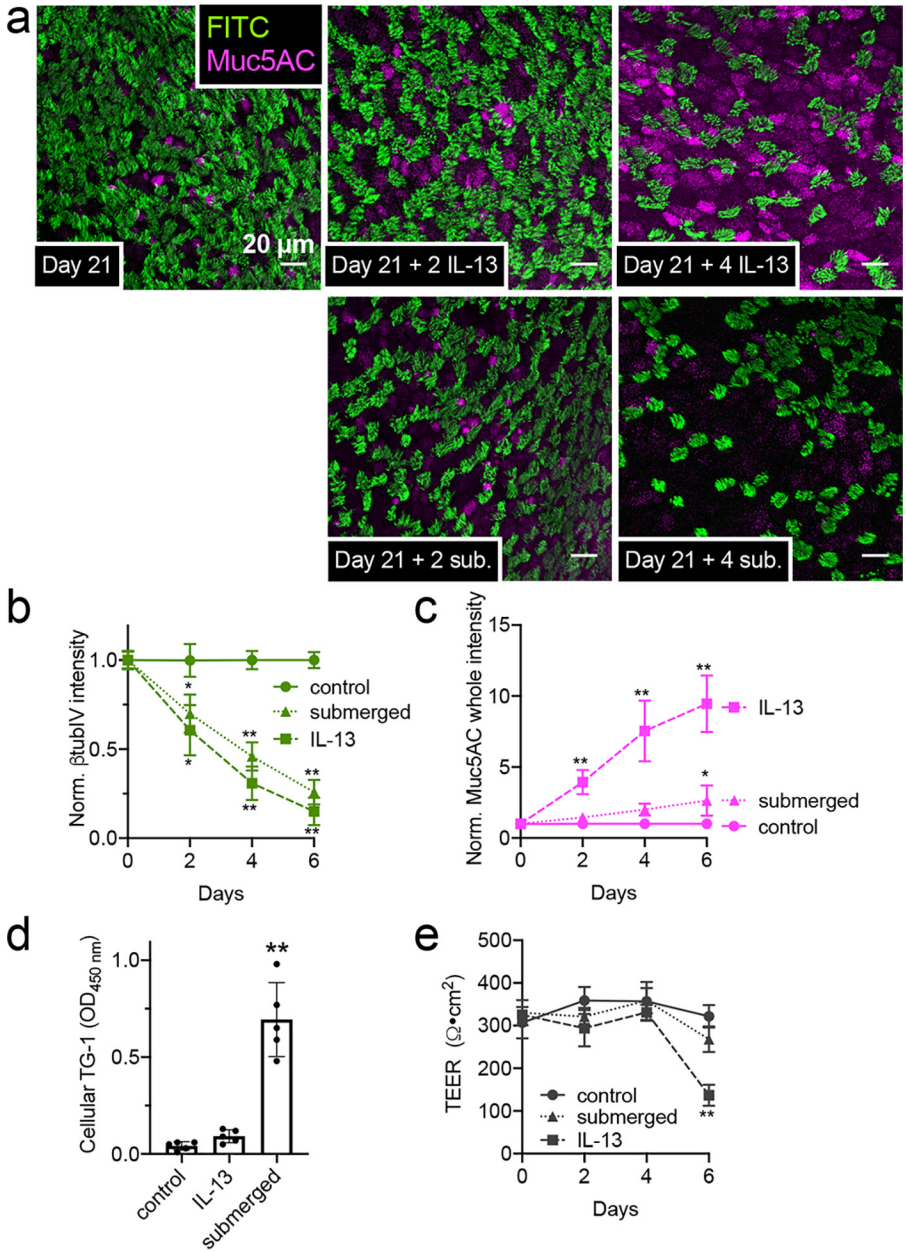

Figure 5. Loss of cilia with IL-13 treatment or submersion of ALI cultures of primary human nasal cells. *a,* representative immunofluorescence (*IF*) of cilia (*β*-tubulin IV; *green)* and Muc5AC (*magenta*) in ALIs 21 days after air (*top left*). *Top, middle*, and *right* show cilia loss after further 2–4 days basolateral IL-13. *Bottom, middle,* and *right* show loss of cilia with less Muc5AC with apical submersion. *b* and *c,* cilia loss (*b*; normalized *β*-tubulin IV IF) and Muc5AC increase (*c*) in cultures (starting at day 21) exposed to subsequent IL-13, apical submersion, or no treatment (*control*). Ten fields from one ALI from one patient were imaged and averaged for an independent experiment; results shown are mean ± S.E. of 4–6 independent experiments (4–6 patients). *d,* squamous marker TG-1 quantified by ELISA at day 25 (21 days at air and then 4 subsequent days of IL-13, submersion, or no treatment). Each data point is an independent ALI from a different patient ($n = 5$ total ALIs). Significance was determined by one-way ANOVA with Dunnett's post-test; **, $p < 0.01$. *e,* TEER at time points as in *b* and *c*. Significance was determined by one-way ANOVA with Bonferroni post-test; *, $p < 0.05$, and **, $p < 0.01$.

the apical response to PAR-2, we tested TGF-β2 secretion and found both basolateral responses and apical responses were blocked by PAR-2 antagonist FSLLRY-NH_2 (Fig. 8*d*).

Impaired ciliogenesis resulting from CSC exposure or retinoic acid deficiency also correlates with altered polarization of PAR-2

The above data suggest that epithelial de-differentiation or remodeling affects the polarization of PAR-2 and may sensitize epithelial cells to protease allergens by allowing apical PAR-2 activation. We tested whether other alterations of epithelial development and ciliogenesis cause this phenotype. We used CSC, shown to inhibit ciliogenesis in nasal ALIs (17). Human ALIs cultured in the presence of 10–30 μg/ml CSC exhibited impaired ciliogenesis at day 20 (Fig. 9, *a* and *b*). Higher concentrations increased epithelial permeability, but barrier function remained intact up to 30 μg/ml CSC (Fig. 9, *c* and *d*). CSC exposure did not affect baseline-resting intracellular calcium concentration ($[Ca^{2+}]_i$, Fig. 9*e*).

On day 20, human nasal ALIs cultured in 10–30 μg/ml CSC, apical 2FLI, Der 3 p, and tryptase induced calcium responses,

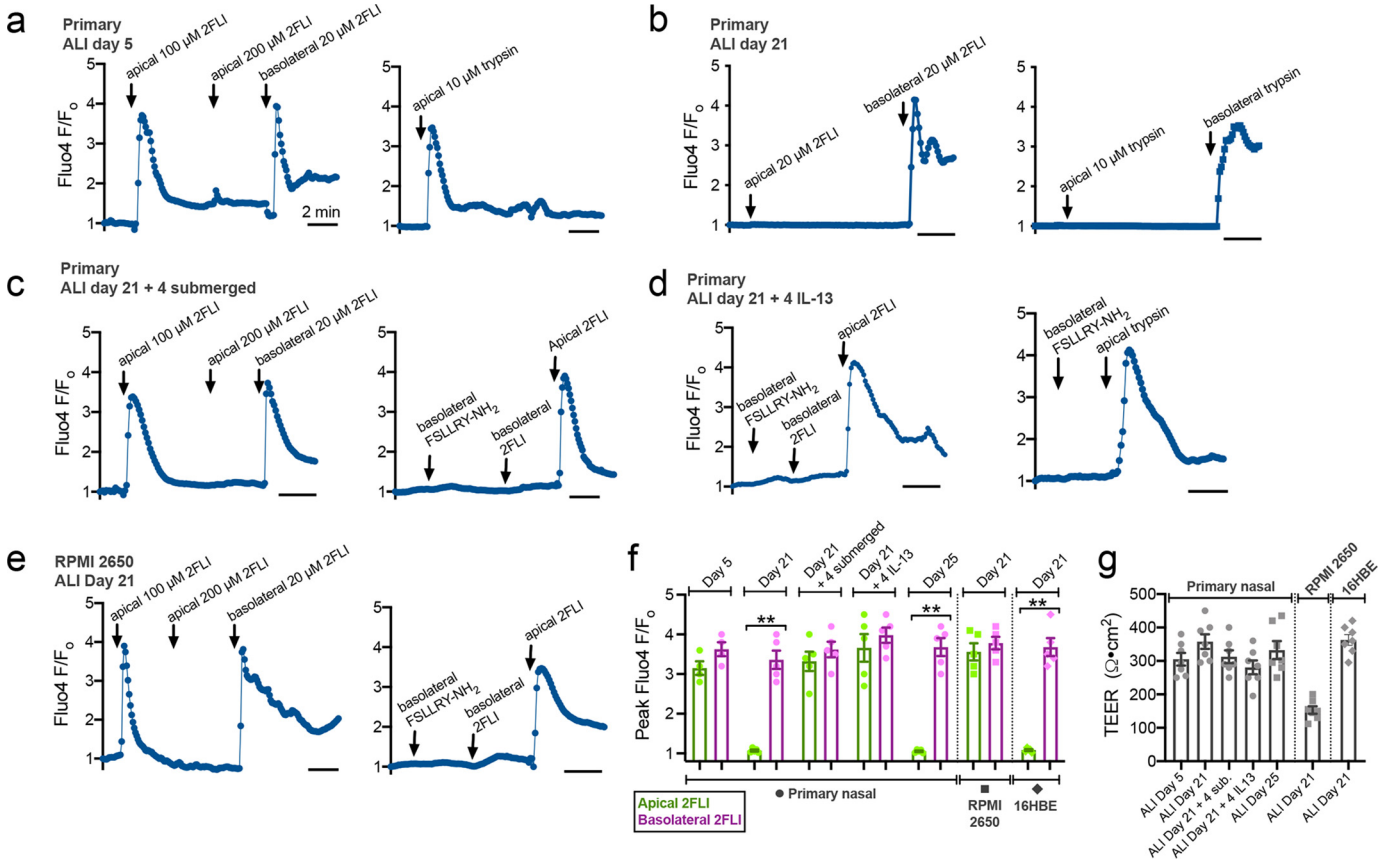

Figure 6. Polarization of PAR-2 signaling in ALIs. *a–d,* primary human nasal ALIs loaded with Fluo-4 were stimulated apically or basolaterally with PAR-2 agonist 2FLI or trypsin. ALIs at day 5 (before ciliogenesis) responded to apical 2FLI (*a*, *left*) or trypsin (*a*, *right*). Basolateral 2FLI elicited further response after apical saturation, suggesting two physically separate PAR-2 pools (*a*, *left*). Responses to apical 2FLI or trypsin were lost by day 21 (*b*) but regained after subsequent 4 days of submersion (*c*) or basolateral IL-13 (*d*). Apical responses to 2FLI were observed even with basolateral PAR-2 antagonist (FSLLRY-NH_2; 100 μM), supporting distinct PAR-2 pools. Representative traces are shown from single ALIs. *e,* RPMI 2650 squamous ALIs exhibited responses to apical 2FLI. Subsequent application of basolateral 2FLI or inhibition of basolateral PAR-2 with FSLLRY-NH_2 also suggest physically separated apical *versus* basolateral PAR-2 pools. *f,* quantification of peak Fluo-4 F/F_o from experiments as in *a–e* (mean ± S.E.; 5–7 experiments using ALIs each different patients). Significance was determined by one-way ANOVA with Bonferroni post-test comparing apical *versus* basolateral 2FLI; **, $p < 0.01$. *g,* TEER from cultures used in *a–f* confirmed 4 days of submersion or IL-13 did not disrupt the epithelial barrier. Significance was determined by one-way ANOVA with Bonferroni post-test.

whereas control cells (0 μg/ml CSC) did not respond (Fig. 9*f*). The apical responses observed in CSC-treated cultures were blocked by the PAR-2 antagonist FSLLRY-NH_2 (Fig. 9*g*). As PAR-2 is partially coupled to inhibitory Gα proteins (Gα_i) that inhibit adenylyl cyclase, we looked at the ability of apical 2FLI exposure to reduce cellular cAMP levels. However, as baseline cAMP levels are low, we co-stimulated ALIs with a low level of adenylyl cyclase–activating compound forskolin (1 μM) to elevate cAMP. We found cAMP was ~50% reduced in CSC-treated but not untreated ALIs with apical exposure to 2FLI or PAR-2 agonist AC 55541, fitting with apical activation of PAR-2 signaling only in CSC-treated cells (Fig. 9*h*). Reductions in cAMP were inhibited by FSLLRY-NH_2 (Fig. 9*h*), demonstrating PAR-2 specificity.

Apical PAR-2 activation also induced TGF-β2 and GM-CSF in human nasal ALIs cultured in 10–30 μg/ml CSC, whereas control cells responded only to basolateral PAR-2 stimulation (Fig. 9*i*). Similar results were observed in mouse ALIs and par-$2^{-/-}$ mice, again confirming that responses to 2FLI were indeed due to PAR-2 (Fig. S9). Together, these data suggest that cigarette smoke-induced alterations of epithelial morphology may change the polarity of PAR-2 in airway epithelial cells well before the onset of full epithelial breakdown. This may contribute to inflammation and disease progression. We next tested another disease-relevant modifier of epithelial differentiation.

The active metabolite of vitamin A, retinoic acid (R.A.), is involved in transcriptional control of ciliogenesis (36, 41, 42). R.A. has anti-allergic effects in mice (43, 44) and *in vitro* cell models. Growing primary airway epithelial cells in the absence of R.A. induces a squamous phenotype (45). Cilia differentiation was measured by acetylated tubulin ELISA in ALIs grown in 50 nM (normal level), 15 nM, or 0 nM R.A. for 20 days. Squamous differentiation was measured by TG-1 ELISA. Retinoic acid reduced cellular TG-1 (Fig. 10*a*), increased acetylated tubulin (Fig. 10*b*), and increased TEER (Fig. 10*c*). R.A.-deficient (15 nM) ALIs exhibited apical 2FLI calcium responses (Fig. 10*d*), whereas R.A.-replete (50 nM) ALIs did not (Fig. 10*d*). Similar results were observed with tryptase and the PAR-2 agonist AC 55541 (Fig. 10*e*). We likewise observed a decrease in cAMP levels with apical exposure to 2FLI only in low (15 nM) R.A. cultures (Fig. 10*f*), while both low (15 nM) and high (50 nM) R.A. ALIs exhibited reduced cAMP with basolateral 2FLI (Fig 10*f*). The apical

2FLI response observed in low R.A. cultures was blocked by FSLLRY-NH_2 (Fig. 10*f*), demonstrating PAR-2 dependence of this effect. Calcium and cAMP responses correlated with GM-CSF secretion at 24 h (Fig. 10*g*). Thus, impairment of ciliogenesis by CSC or reduced R.A. can both alter epithelial polarity of PAR-2 signaling.

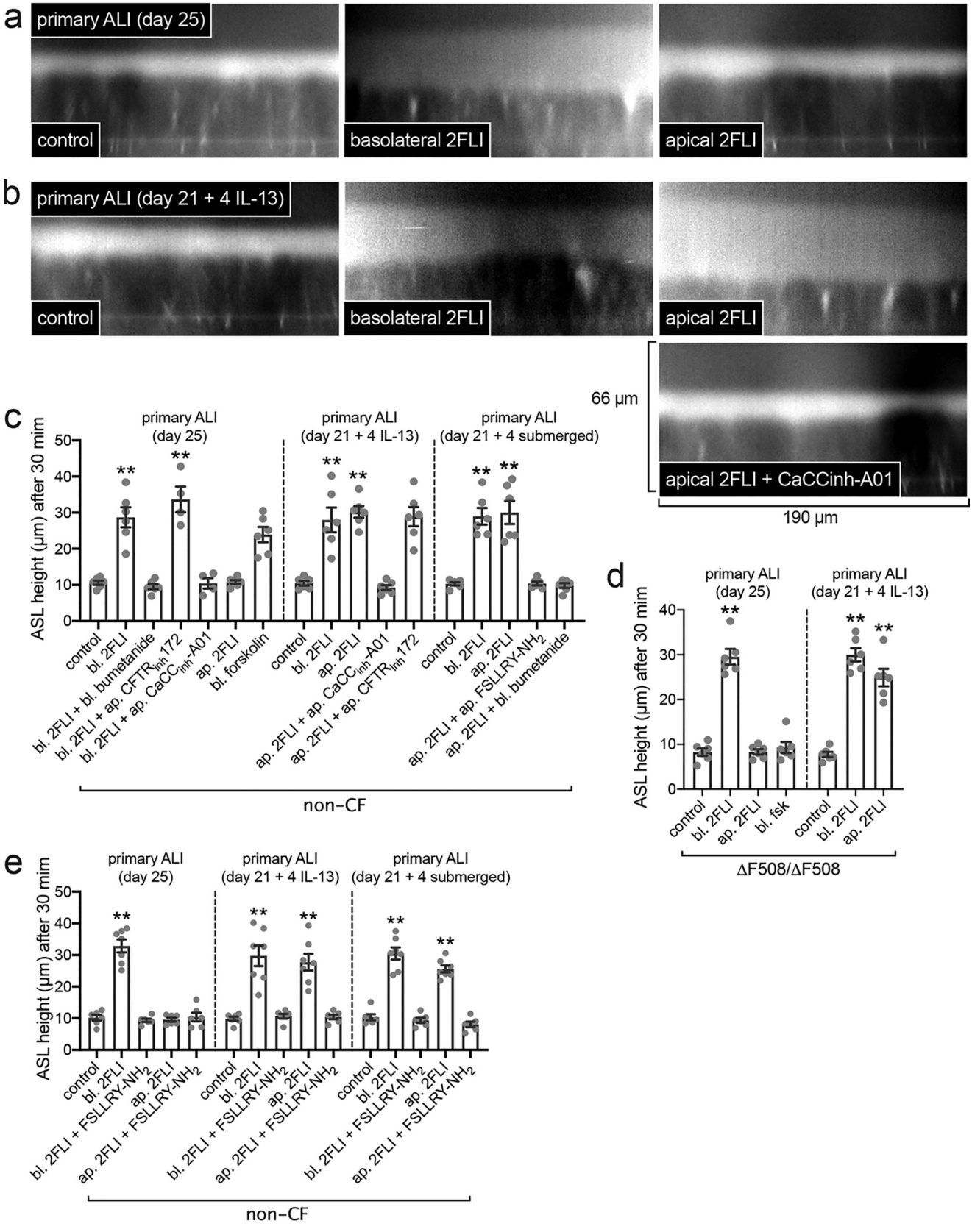

Patient tissue explants from polyps, but not control turbinate, exhibit apical PAR-2 responses

To further test whether epithelial remodeling observed in airway diseases translates to altered PAR-2 responses, we took tissue explants from nasal polyps, removed from CRS patients during functional endoscopic sinus surgery, and control middle turbinate tissue, removed from patients during surgery for other indications (*e.g.* trans-nasal approaches to the skull base to remove pituitary tumors). Tissue was mounted, imaged by confocal microscopy, and stimulated apically with PAR-2 agonists. Polyp tissue exhibited apical responses to 2FLI, trypsin, or Der p 3, but not thrombin (Fig. 11, *a* and *b*). Control uninflamed middle turbinate tissue did not (Fig. 11*c*). Data are summarized in (Fig. 11*d*). The apical responses to PAR-2 agonists 2FLI or SLIGRL-NH_2 in polyp tissue were inhibited by PAR-2 antagonist FSLLRY-NH_2 (Fig. 11*e*). Scrambled agonist peptide LRGILS-NH_2 had no effect on Ca^{2+} (Fig. 11*e*).

Immunofluorescence revealed that PAR-2 was nonetheless basolaterally expressed in ciliated cells from nasal polyps (Fig. 11*f*), as we previously reported for nonpolyp tissue (8). Moreover, the calcium responses to PAR-2 stimulation were not enhanced in isolated polyp *versus* turbinate ciliated cells (Fig. 11*g*). We thus hypothesized that apical PAR-2 responses do not originate from within the ciliated cells themselves, but rather may occur through de-differentiation and/or remodeling of the epithelium toward a more squamous phenotype.

Apical PAR-2 stimulation requires intercellular communication to increase ciliary beat frequency

To test whether ciliated cells autonomously respond to apical PAR-2 stimulation, we measured CBF to apical PAR-2 agonists in control and IL-13–treated cultures. We combined CBF measurement with two structurally-distinct gap junction inhibitors, steroid-like small molecule inhibitor carbenoxolone (CBX) and peptide inhibitor Gap 27 (46). Control cultures exhibited CBF increases with basolateral but not apical 2FLI; basolateral responses were unaffected by CBX (Fig. 12, *a*, *b* and *g*). IL-13–treated cultures exhibited CBF increase with apical 2FLI (Fig. 12*c*) inhibited by CBX or Gap 27 (Fig. 12, *d*–*g*). Basolateral 2FLI responses were not inhibited by CBX (Fig. 12*g*). Apical ATP responses were inhibited by neither CBX nor Gap 27 (Fig. 12*g*). These data support a model by which well-differentiated airway epithelial tissue (Fig. 12*h*) expresses basolateral PAR-2 within ciliated cells, as CBF increases do not require intercellular gap junction communication (Fig. 12*h*). However, dedifferentiation of the epithelium results in apical expression of PAR-2 within nonciliated cells that can increase CBF in ciliated cells only in the presence of functional gap junctions, likely to allow diffusion of calcium and/or inositol 1,4,5-trisphosphate (Fig. 12*i*).

Discussion

Prior literature on PAR-2 in the airway has focused on increased PAR-2 expression in inflamed airway mucosa (2, 38, 47). However, we show that a potentially important overlooked consideration is the polarity of PAR-2 signaling, which can change in the absence of PAR-2 expression level changes and in the absence of epithelial barrier breakdown. This may represent a novel mechanism by which the airway epithelium can become responsive to apical exposure to inspired/inhaled proteases such as dust mite or *Alternaria* proteases. Our study suggests that changes in airway epithelial composition can have marked effects on polarity even before the basolateral membrane becomes accessible with epithelial breakdown. Such processes may contribute to the early pathogenesis of inflammatory airway diseases even before chronic inflammation and reduced barrier function.

We also confirm previous observations that PAR-2 is a player in detection of *A. fumigatus* using an optical assay that can detect PAR-2 activation independent of other effects *A. fumigatus* conditioned media may have. Furthermore, we defined mechanisms of PAR-2 inflammation and fluid secretion in well-differentiated sinonasal cells cultures at ALI. Although previous studies have suggested PAR-2 activation can stimulate fluid secretion that involves CFTR (48, 49), we only observed CaCC-dependent secretion, suggesting this pathway would not be altered in patients with CF due to loss of CFTR function.

Our data suggest that such alterations of epithelial morphology and composition due to inflammation, exposure to toxic compounds, or other environmental factors can all alter PAR-2 polarity (Fig. 13). This may occur through increased Th_2 cytokines, cigarette smoke exposure, or vitamin A deficiency. Exposure to inhaled allergens like dust mite or fungal proteases may normally be tolerated in healthy airway tissue if these allergens are cleared by mucociliary clearance before they can degrade the epithelial barrier and activate basolateral PAR-2. Moreover, airway submucosal gland secretions contain a variety of protease inhibitors that could neutralize pathogen proteases upon contact with mucus (50, 51). However, in some obstructive airway diseases, altered polarization of PAR-2 may combine with impaired protease inhibitor secretion due to gland duct plugging often observed (52–54). These phenotypes may result in epithelial sensitization to proteases at the apical membrane, increasing inflammatory responses.

Figure 7. Epithelial remodeling is associated with enhanced fluid secretion to apical PAR-2 stimulation. *a,* representative orthogonal confocal sections of control cultures with Texas Red dextran-labeled ASL showing increase in ASL height (reflecting fluid secretion) with basolateral but not apical 2FLI (~25 μM). *b,* representative sections of IL-13–treated cultures showing increased secretion with either basolateral or apical 2FLI and inhibition by the CaCC inhibitor $CaCC_{inh}$-A01 (~10 μM). *c,* peak ASL heights from independent experiments, each the average of 10 ASL measurements from one ALI; there were six experiments per condition. Note no inhibition of secretion with $CFTR_{inh}172$ (~10 μM), but there was inhibition with NKCC1 inhibitor bumetanide (100 μM) or PAR-2 antagonist FSLLRY-NH_2 (~10 μM). Drugs applied to the apical (*ap.*) side were sonicated in perfluorocarbon to not disturb the aqueous ASL layer; thus, apical concentrations are approximate. *d,* data experiments using ΔF508/ΔF508 homozygous CF ALIs. Note no response in CF cultures to basolateral (*bl.*) forskolin (20 μM), which elevates cAMP and activates CFTR (non-CF cultures responded in *c*). Each point is an independent experiment using cells from one patient (five patients total). *e,* experiments similar to *c* were performed ± PAR-2 antagonist FSLLRY-NH_2 to demonstrate PAR-2 specificity of the response in both apical and basolateral 2FLI exposure. Each point is an independent experiment using an ALI culture from one patient (four to six ALIs from four to six patients per condition). Significance was determined in *c*–*e* by one-way ANOVA with Dunnett's post-test; **, $p < 0.01$ *versus* control (*no stim*) for each condition.

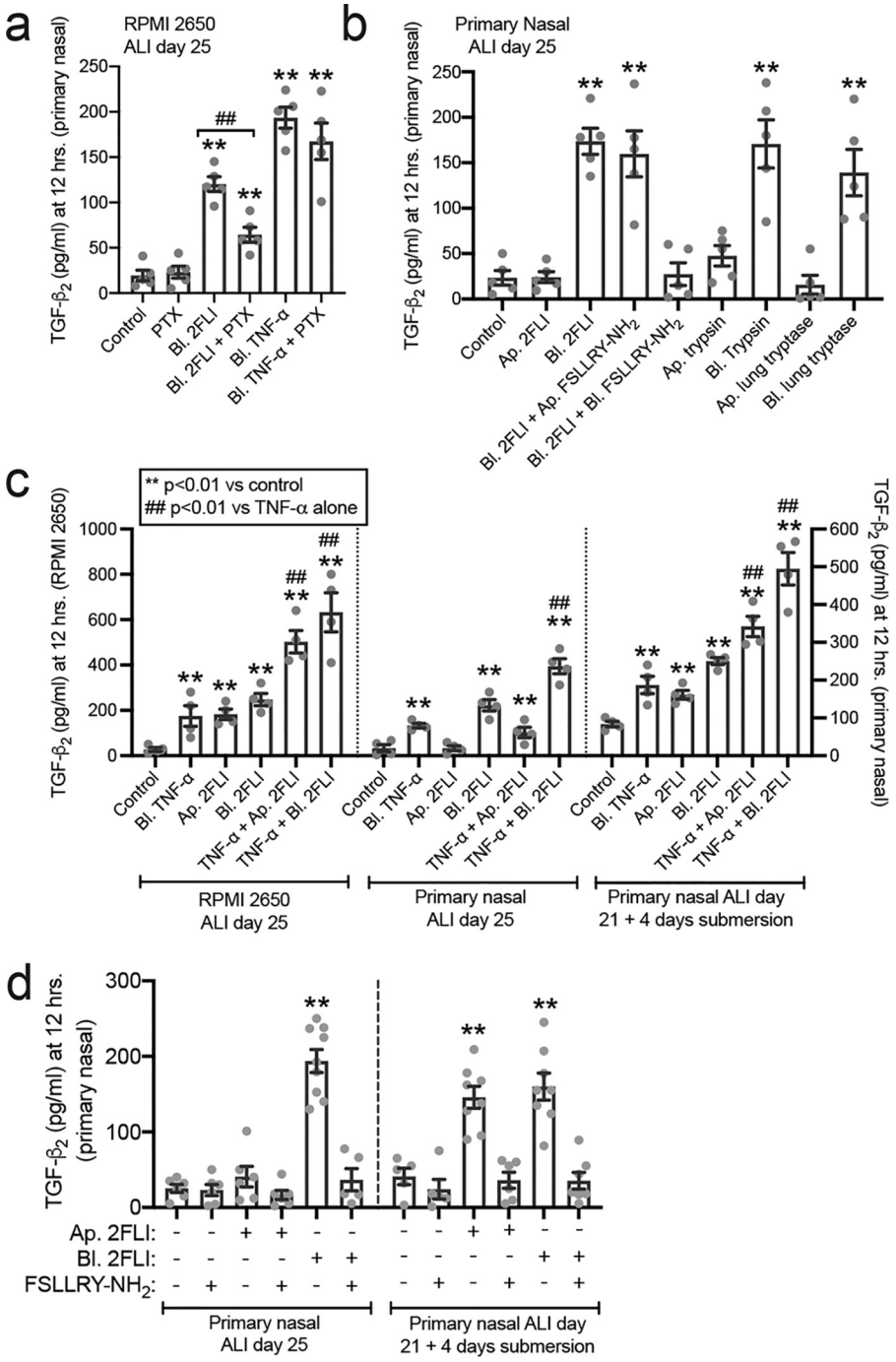

Figure 8. Altered PAR-2 polarity translates to altered TGF-β2 secretion with PAR-2 stimulation both alone and in combination with TNFα. *a, bar graph* of RPMI 2650 ALI TGF-β2 secretion with basolateral (*bl.*) application of 2FLI (20 μM) or TNFα (10 ng/ml) ± pertussis toxin (100 ng/ml; 18 h pretreatment). *b, bar graph* of primary nasal ALIs showing TGF-β2 secretion with basolateral (*bl.*) but not apical (*ap.*) 2FLI (20 μM), trypsin (10 nM), or tryptase (10 nM). *c, bar graph* showing TGF-β2 secretion with apical *versus* basolateral 2FLI and combinatorial effects with TNFα. RPMI 2650 squamous ALIs and primary ALIs exposed to 4 days of submersion to induce squamous differentiation exhibited apical 2FLI responses but control ALIs did not. *d, bar graph* showing TGF-β2 secretion with apical *versus* basolateral 2FLI as in *b* ± FSLLRY-NH_2 (50 μM). Each *point* is an independent experiment using an ALI culture from one patient (four to six ALIs from four to six patients per condition). Significance was determined in *a–d* by one-way ANOVA with Dunnett's post-test comparing values to the respective control; **, $p < 0.01$. *a*, ##, $p < 0.01$ between basolateral 2FLI and 2FLI with PTX by one-way ANOVA with Bonferroni post-test. *c*, ##, $p < 0.01$ *versus* TNFα alone by one-way ANOVA with Bonferroni post-test.

Squamous de-differentiation is a commonly-observed histological finding in CRS patients (19, 20), CF patients (55), or smokers (16, 56). Squamous metaplasia also occurs during epithelial injury and repair (15). Prior studies have focused on the loss of ciliated cells and resulting reduced mucociliary clearance, but we show here that introduction of squamous cells into the epithelium can alter airway epithelial signaling, including an increase in apical PAR-2 responsiveness. This suggests disruption of the normal epithelial composition during disease has physiological consequences beyond reduced mucociliary clearance.

RPMI 2650 cells were proposed as a model of nasal permeability for drug transport studies (57, 58) and cytokine release in

allergy (59) or viral infection (60). Our data here suggest that RPMI 2650 PAR-2 polarization is similar to squamous epithelial cells but not the same as well-differentiated ciliated cells, so interpretation of RPMI 2650 studies should be done cautiously. Altered polarization may extend to multidrug resistance proteins or other transporters or channels relevant for epithelial absorption. RPMI 2650 studies might not reflect healthy sinonasal epithelium but may reflect inflamed remodeled epithelium such as polyp tissue.

Topical long-lasting PAR-2 antagonists might be useful in CRS patients with fungal or dust mite–activated allergic rhinitis by limiting apical PAR-2 activation, particularly if antagonists

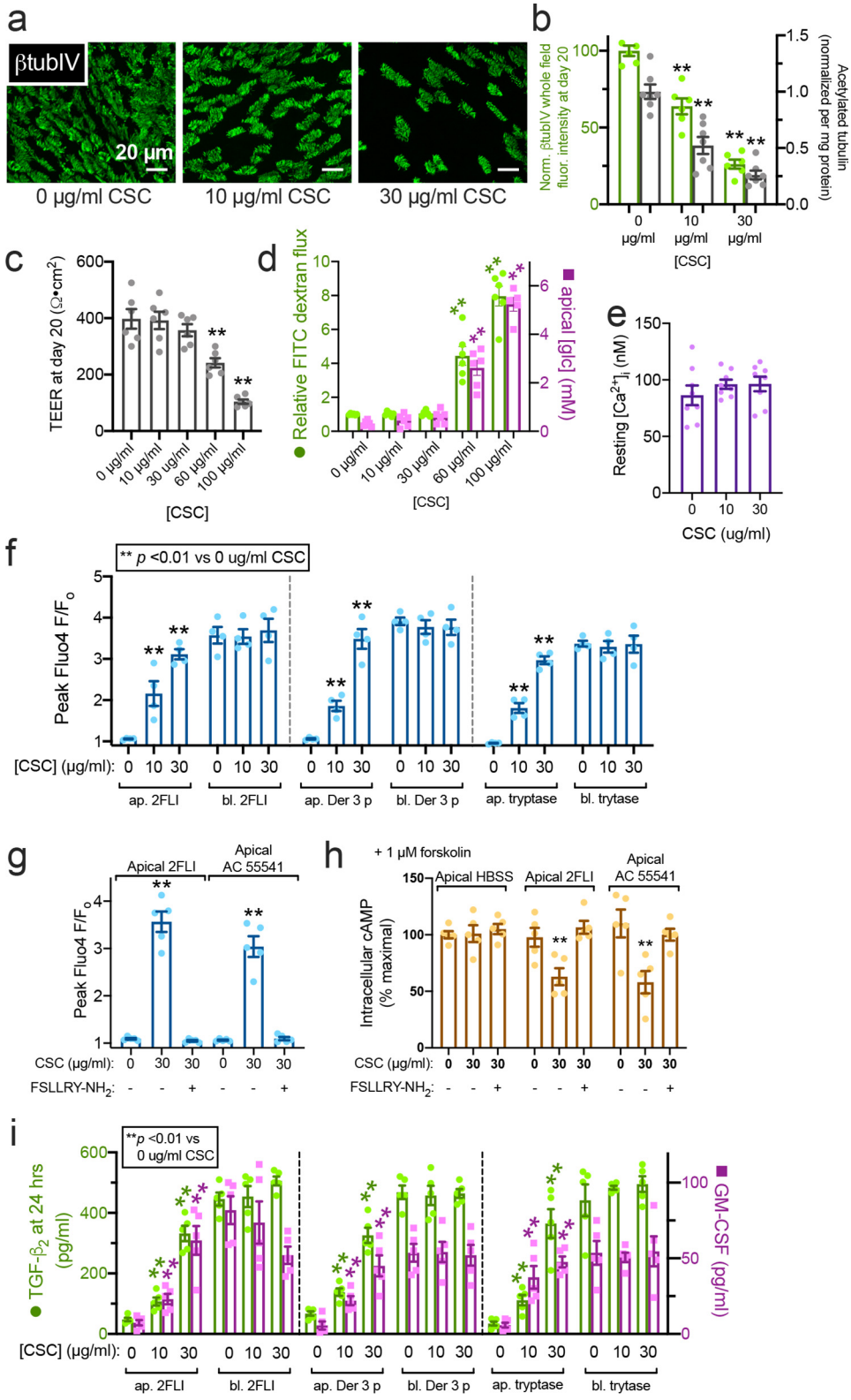

could be designed to not cross the epithelial barrier and block basolateral PAR-2 (*e.g.* a dextran conjugate), and delivered via topical nasal rinse. Such antagonists delivered via inhaler may be similarly useful in patients with allergic asthma. This requires further investigation to test the clinical utility of this strategy. Alternatively, restoring a normal differentiated epithelial phenotype by reducing inflammation may lower the epithelial sensitivity to proteases.

Experimental procedures

Reagents and materials

Fluo-4, CellRox, Texas Red dextran, FITC dextran, and Alexa Fluor-labeled secondary donkey anti-mouse and donkey anti-rabbit were from Thermo Fisher Scientific (Waltham, MA). PAR-2 antibodies SAM-11 (mouse monoclonal) and EPR180953 (rabbit monoclonal), Na^+/K^+-ATPase (EP1845Y; rabbit monoclonal), and Glut1 (SPM498; mouse monoclonal) were from Abcam (Cambridge, UK). PAR-2 agonist peptide SLIGKV-NH_2 (H-4624) and scrambled LSIGKV-NH_2 (catalog no. H-6428) were from Bachem (Torrance, CA). LDH assay kit (catalog no. ab65393) and 2-furoyl-LIGRLO-NH_2 (2FLI; catalog no. ab120800) were from Abcam. Glucose assay kit (catalog no. 10009582), XTT assay kit (catalog no.10010200), and MTT assay kit (catalog no.10009365) were from Cayman Chemical (Ann Arbor, MI).

Multiple PAR-2–activating agonists were used in this study to ensure results were not an artifact of any one peptide or protease. PAR-2 antagonist FSLLRY-NH_2 (catalog no. 4751/1), PAR-2 agonist SLIGRL-NH_2 (catalog no. 1468/1; EC_{50} 5 μM), scrambled LRGILS-NH_2 (catalog no. 3394/1), PAR-4 agonist AY-NH_2 (catalog no. 1487/1), and PAR-4 antagonist tcY-NH_2 (catalog no. 1488) were from Tocris (Bristol, UK). AC 55541, a small molecule PAR-2 agonist ($EC_{50} = 6–7$ μM), and AZ3451, a small molecule PAR-2 allosteric antagonist, were from Cayman Chemical (catalog nos. 17736 and 29671, respectively). Recombinant Der p 3 (catalog no. MBS1096978) was from MyBioSource (San Diego, CA). ELISAs for GM-CSF (900-K30) and IL-6 (900-K16) were from PeproTech (Rocky Hill, NJ). Human TGFβ2 ELISA (DB250) and mouse TGFβ2 DuoSet ELISA (DY7346–05) were from R&D Systems (Minneapolis, MN). Transglutaminase 1 (TG-1) ELISA (OKCD01601) was from Aviva Systems Bio (San Diego, CA). Acetylated tubulin ELISA (catalog no. 7204) was from Cell Signaling Technologies (Danvers, MA). Cigarette smoke condensate was a gift from Noam Cohen (University of Pennsylvania), originally purchased from Murty Pharmaceuticals, Inc. (Lexington, KY; Batch R041018) as stock 40 mg/ml in DMSO stored at −80 °C. Unless indicated below, all other regents were from Sigma-Aldrich.

Cell line culture

Cell line culture was as described previously (8, 61, 62). Briefly, RPMI 2650 and NCI–H520 squamous cells as well as BEAS-2B and A549 cells were obtained from ATCC (Manassas, VA). 16HBE cells (SV-40 immortalized normal human bronchia) were obtained from D. Gruenert (University of California San Francisco, San Francisco). Cells were grown in submersion in Minimal Essential Media with Earle's salts (Gibco; Gaithersburg, MD) supplemented with 10% FetalPlex (GeminiBioproducts; West Sacramento, CA) and 1% penicillin/streptomycin mix (Gibco). RPMI 2650 and 16HBE cells were seeded for ALI culture onto Corning transwells (0.3-cm^2 surface area; 0.4-μm pore size) (Corning, NY) and grown for 5 days in the above media to confluence. Upon apical exposure to air, the basolateral medium was switched to primary cell differentiation media indicated below. ALIs were fed three times weekly. Transfection of submerged BEAS-2B and A549 cells was carried out in 8-well chamber slides (CellVis) with Lipofectamine 3000 as described previously (61).

XTT assays were carried out as described in the manufacturer's instructions using phenol-free DMEM (5.5 mM Glc; Gibco). Changes in XTT fluorescence were measured in real time in a Tecan Spark 10M plate reader equipped with heating (37 °C) and gassing (5% CO_2). Technical replicates were used to ensure the reliability of single values. Experimental replicates presented in the text are independent experiments performed on different days with different batches of cells. PAR-2 immunofluorescence, biochemistry, and molecular biology in squamous cell lines were carried out as described for primary cells (8).

Fungal culture

Fungal culture was carried out as described previously (63). Briefly, cultures of *A. niger* (strain WB326 (ATCC16888), *A. fumigatus* NIH5233 (ATCC 13073), and NRRL163 (ATCC1022)) were grown by the Clinical Microbiology Lab, Philadelphia Veterans Affairs Medical Center, in 40 ml of BACTEC Myco/F Lytic Culture Vials (BD Biosciences) at 30 °C for 10 days. CM was then extracted and filtered sequentially through 0.45- and 0.2-μm filters as described previously (63). Aliquots of CM were flash-frozen and stored at −80 °C and thawed immediately before use. For calcium-imaging experiments, fungal CM was dialyzed overnight (Spectra/Por 1 regenerated cellulose

Figure 9. Impaired ciliation by CSC exposure alters PAR-2 polarity. *a,* representative image showing reduction of cilia in ALIs exposed to CSC. *b,* quantification of β-tubulin IV immunofluorescence (*green*) and ELISA measurement of acetylated tubulin (*gray*). *c,* TEER from cultures exposed to CSC for 20 days of ALI differentiation; 30 μg/ml reduced cilia but maintained TEER. *d,* FITC–dextran permeability and apical glucose concentration with CSC, confirming barrier integrity at ≤30 μg/ml CSC. *e, bar graph* showing no statistically significant difference in resting intracellular calcium concentration $[Ca^{2+}]_i$ in cultures treated with 0, 10, and 30 μg/ml CSC as in *b–d*. Significance was tested with one-way ANOVA with Bonferroni post-test. *f,* peak calcium responses to apical (*ap.*) and basolateral (*bl.*) 2FLI (25 μM), Der 3 p (1 μM), and tryptase (1 μM) in ALIs with 0, 10, or 30 μg/ml CSC. Note increase of apical 2FLI responses with increased CSC. *g, bar graph* showing apical responses to 2FLI or AC 55541 after CSC exposure were inhibited by PAR-2 antagonist FSLLRY-NH_2. *h,* decreases in cAMP during apical PAR-2 stimulation (50 μM 2 FLI or 20 μM AC 55541 ± 100 μM PAR-2 antagonist FSLLRY-NH_2 for 10 min) in ALIs treated with 0 or 30 μg/ml CSC as in *b–g* were quantified by ELISA. As baseline cAMP levels were too low to quantify by this method, cultures were treated concomitantly with 1 μM adenylyl cyclase–activating compound forskolin to elevate cAMP high enough for measurement. *i,* TGF-β2 and GM-CSF were measured by ELISA after 24 h apical or basolateral stimulation as in *e*. Note increased cytokine secretion with apical 2FLI in ALIs exposed to CSC. Significance was determined in *b–g* and *i* determined by one-way ANOVA with Bonferroni post-test comparing each value to its respective 0 CSC control; **, $p < 0.01$. Data points are from 6 to 10 individual ALIs from three to five human patients.

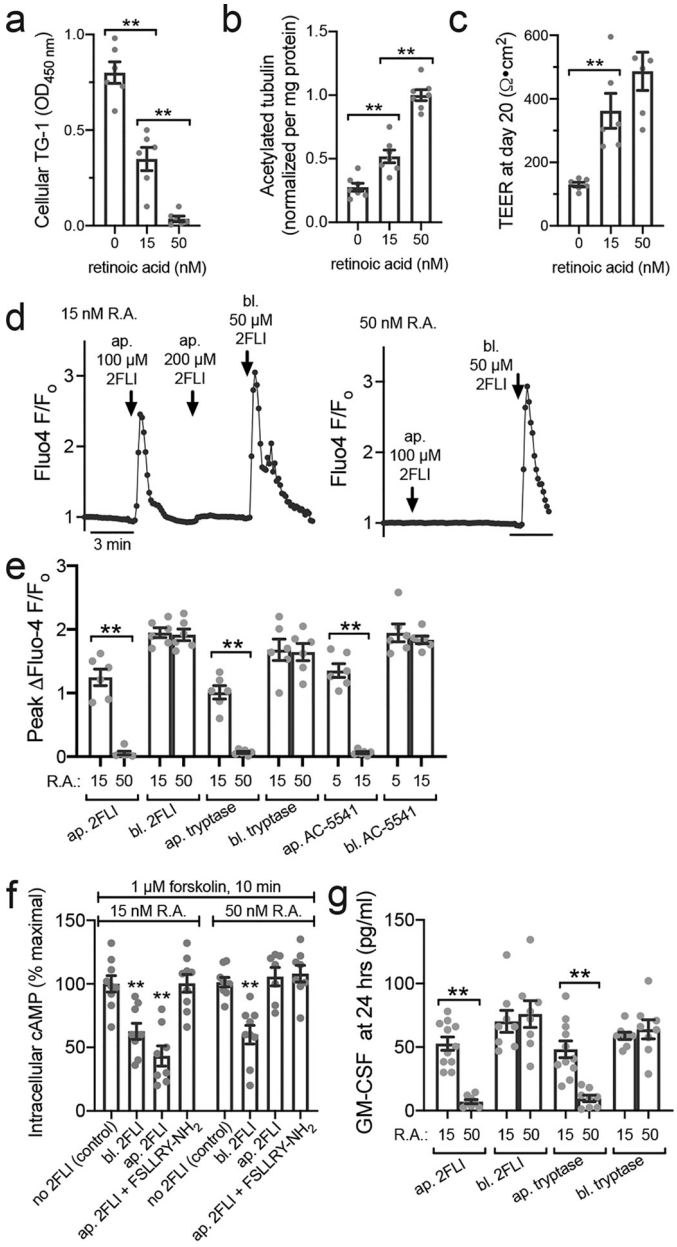

Figure 10. R.A. deficiency also alters PAR-2 polarity. *a, bar graph* showing cellular TG-1 increase in primary human ALIs grown with reduced R.A. *b, bar graph* showing cellular acetylated tubulin reduction with decreased R.A. *c, bar graph* showing lower TEER measurements in the absence of R.A. No significant difference was observed between 15 and 50 nM R.A. *d,* representative Fluo-4 traces showing apical 2FLI response in low R.A. (15 nM) but not normal R.A. (50 nM) culture. Note in *left trace* that basolateral 2FLI increased calcium even after saturating apical 2FLI, supporting two pools of PAR-2 separated by the epithelial barrier. *e,* peak change in Fluo-4 F/F_o with apical (*ap.*) *versus* basolateral (*bl.*) 2FLI (50 μM), tryptase (10 μM), or PAR-2 agonist AC 55541 (10 μM) in cultures grown in 15 or 50 nM R.A. *f,* decreases in cAMP during apical *versus* basolateral PAR-2 stimulation (50 μM) were quantified by ELISA. As baseline cAMP levels were too low to quantify by this method, cultures were treated concomitantly with 1 μM adenylyl cyclase–activating compound forskolin ± 2FLI as indicated. Significance was determined by one-way ANOVA with Bonferroni post-test comparing all *bars* with control (no 2FLI) at either 15 or 50 nM R.A.; **, $p < 0.01$. *g,* GM-CSF was measured by ELISA after apical or basolateral stimulation with 2FLI (10 μM) or tryptase (20 nM). Note responses were observed to apical stimulation in *e* and *f* only in cultures with low R.A. All data points are independent experiments (6–10 per condition) using ALIs cultured from three to six patients (two ALIs per patient). Significance was determined by one-way ANOVA with Bonferroni post-test; **, $p < 0.01$.

6–8-kDa MWCO tubing) at 4 °C against an ~500× volume of HBSS to remove small molecules and equilibrate salt concentrations.

PAR-2 Trio assay

PAR-2 Trio assay was modified from Ref. 26. Vectors for PAR-2 and β2 adrenergic receptor Trio assays were from Xiaokun Shu via Addgene. Cells were co-transfected with two pcDNA3 plasmids encoding the GFP β-strands 1–9 (Addgene catalog no. 121684) and a pcDNA3 plasmid expressing the receptor fused to GFP β-strand 11, an arrestin fused to GFP β-strand 10, and mCherry as a transfection marker (Addgene catalog no. 113609 or 113610) and imaged 24 h after transfection at room temperature using standard GFP and TRITC filters on an Olympus IX83 microscope with ×40 (0.75NA PlanFluor) objective. Sapphire CKAR or Sapphire CKAR(T/A) (64) was from Jin Zhang via Addgene (catalog nos. 118468 and 118469) and was imaged using the 380 nm channel of a fura-2 filter set (Chroma Technologies, Rockingham, VT).

Generation of primary sinonasal ALI cultures from residual surgical material

Primary human sinonasal cell culture was carried out as extensively described (8, 61, 62, 65). Tissue acquisition was carried out in accordance with University of Pennsylvania guidelines regarding the use of residual clinical material, using tissue from patients ≥18 years of age undergoing surgery for sinonasal disease (CRS), or other procedures (*e.g.* trans-nasal approaches to the skull base). Institutional review board approval (no. 800614) and written informed consent was obtained in accordance with the United States Department of Health and Human Services code of federal regulation Title 45 CFR 46.116 and the Declaration of Helsinki. Clinical information regarding patient samples is listed in Table S1.

Human sinonasal epithelial cells were enzymatically dissociated and grown to confluence in 50% DMEM/Ham's F-12 plus 50% bronchial epithelial basal media (BEBM, Lonza) for 7 days (8, 61, 62). Dissociated cells were then seeded on Transwell filters (Corning) coated with type I bovine collagen, fibronectin, and BSA. Culture medium was removed from the upper compartment after 5–7 days, and cells were fed basolaterally with differentiation medium containing 50% DMEM and 50% BEBM plus Lonza B-ALI Singlequot hEGF (0.5 ng/ml), epinephrine (5 ng/ml), bovine pituitary extract (0.13 mg/ml), hydrocortisone (0.5 ng/ml), insulin (5 ng/ml), triiodothyronine (6.5 ng/ml), and transferrin (0.5 ng/ml), supplemented with 100 units/ml penicillin, 100 μg/ml streptomycin, 0.1 nM retinoic acid (B-ALI inducer; added fresh for each feeding) as described. For ELISA measurements of ALI culture lysate, a lysis buffer containing no SDS was used, containing 150 mM NaCl, 1 mM EDTA, 0.3% Triton X-100, 0.3% Tween 20, and 100 mM Tris, pH 7.4, with Complete Protease Inhibitor mixture (Roche Applied Science). All lysates were normalized by addition of excess lysis buffer to a protein concentration of 2 mg/ml, measured using a Bio-Rad DC protein assay.

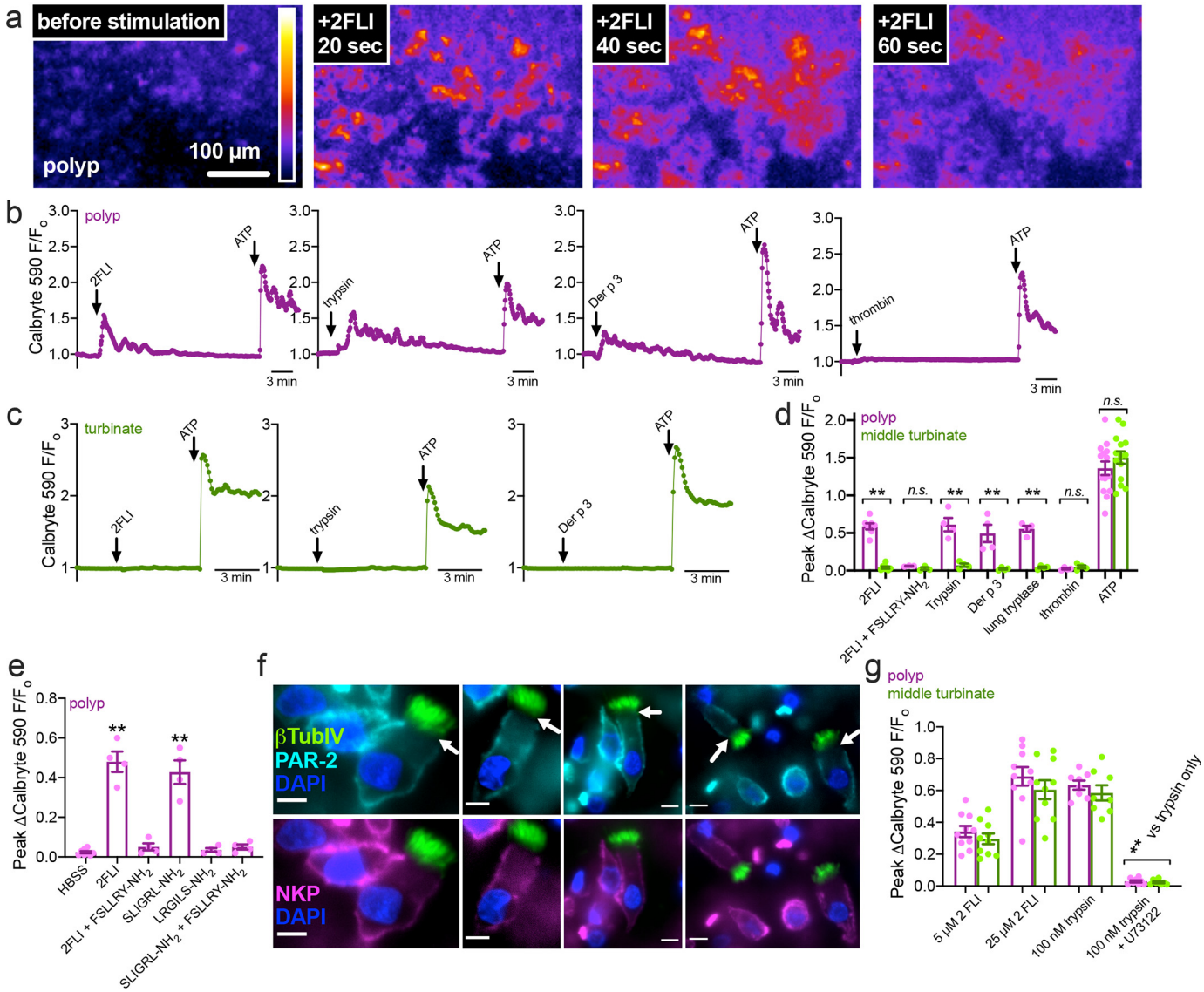

Figure 11. Nasal polyp exhibited calcium responses to apical PAR-2 stimulation but control turbinate did not. *a*, representative image of 2-FLI induced calcium response (Calbryte 590) in a thin piece of polyp mucosa mounted in an Ussing chamber holder and imaged with a spinning disk confocal microscope. *b* and *c*, representative traces of polyp (*b*) and turbinate (*c*) responses to apical 2FLI (50 μM), trypsin (1 μM), Der p 3 (1 μM), or thrombin (1 μM). ATP (100 μM), which activates apical purinergic receptors, was a positive control. *d*, peak change in calcium in tissue treated apically with PAR-2 agonists. Each data point is an independent experiment using tissue from separate patients ($n = 7$ per condition). *e*, peak change in calcium in polyp tissue treated apically with PAR-2 agonist (50 μM 2FLI or 120 μM SLIGRL-NH_2) ± antagonist (80 μM FSLLRY-NH_2), confirming responses are due to PAR-2. Each data point is an independent experiment using tissue from separate patients ($n = 4$ per condition). *f*, immunofluorescence showing lack of apical PAR-2 staining in polyp ciliated cells with Na^+K^+ ATPase (*NKP*) as marker for the basolateral membrane and β-tubulin IV (*βTubIV*) (cilia marker) shown in *green*. Pearson's correlation and Mander's overlap coefficients for NKP and PAR-2 in ciliated cells were both ≥0.95 in 10 images analyzed. *Scale bars* are 10 μm. *g*, peak change in calcium in isolated ciliated cells; *n.s.*, no significant difference was observed between polyp and turbinate. Significance in *d* and *g* was determined by one-way ANOVA with Bonferroni post-test and significance in *e* by one-way ANOVA with Dunnett's post-test comparing all values to HBSS only control; **, $p < 0.01$.

Generation of mouse nasal septum ALIs

Experiments using primary mouse nasal septal ALI cultures utilized residual tissue from mice euthanized for other experimental purposes according to the "Guide for the Care and Use of Laboratory Animals" (Institute of Laboratory Animal Resources, National Research Council) with institutional approval. Cell culture was carried out as described.

Nasal septum was removed from C57BL/6J Wt and PAR-2 knockout (B6.Cg-*F2rl1*^{tm1Mslb}/J; The Jackson Laboratory, Bar Harbor, ME) mice euthanized for other experimental purposes with IACUC approval according to National Institutes of Health guidelines, the principles of ARRIVE, and the Basel Declaration. No animals were sacrificed solely for the experiments in this study. Nasal septum was dissociated and cultured at air–liquid interface, as described previously (8), and used after 3 weeks' exposure to air for full differentiation in DMEM/F12K media containing 2% NuSerum (Corning), 100 units/ml penicillin, 100 μg/ml streptomycin.

qPCR

RNA was isolated from ALI cultures or stripped turbinate or polyp epithelium, as described previously (46), and qPCR was performed using TaqMan primers (Thermo Fisher Scientific) for F2RL1 (Hs00608346_m1), ACTB (Hs01060665_g1), and

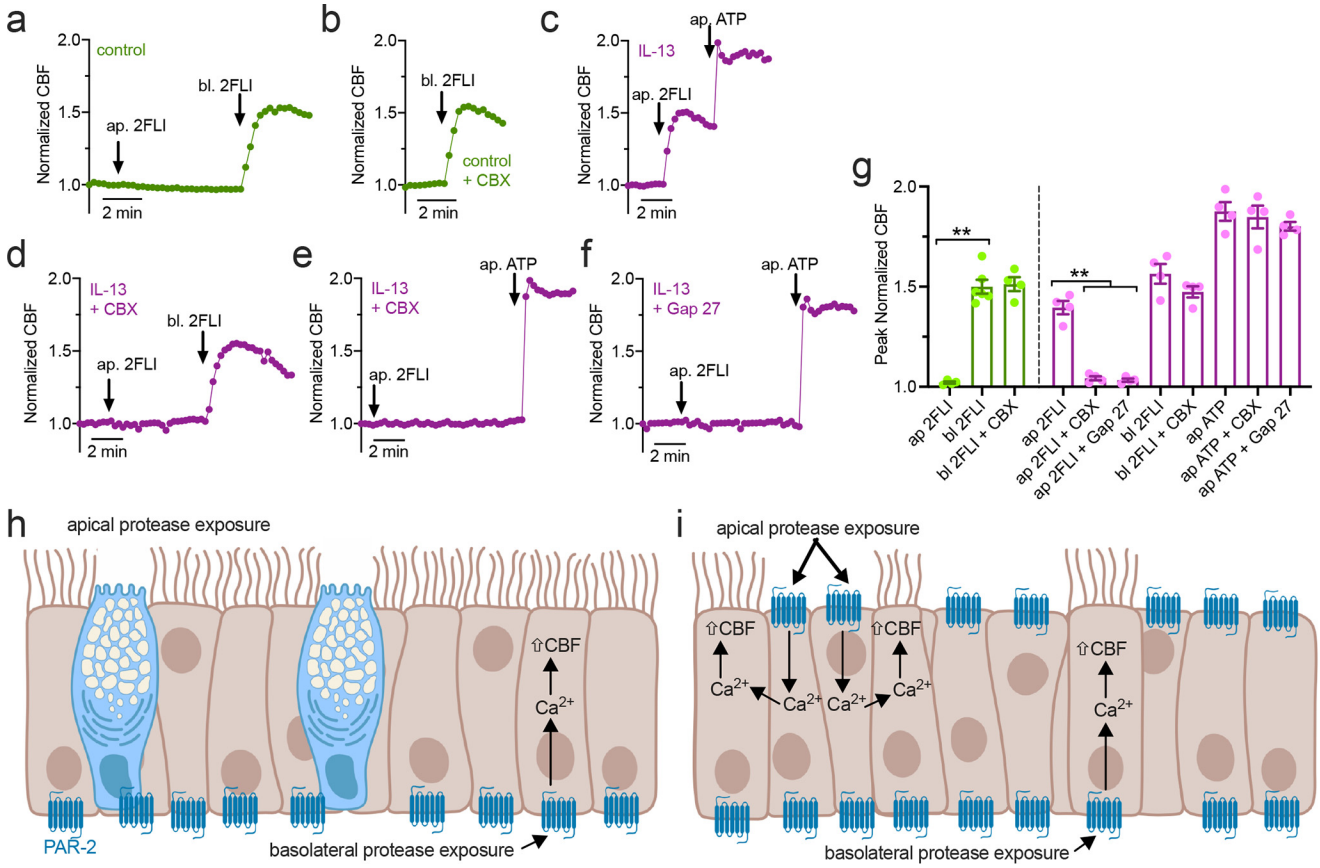

Figure 12. CBF measurements of nasal epithelial cells exposed to apical or basolateral 2FLI. *a* and *b,* representative traces of CBF with 2FLI ± carbenoxolone (100 μM; 30 min preincubation). Control cultures (day 25 at ALI) exhibited no increased CBF with apical (*ap.*) 2FLI application but an ~50% increase in CBF with basolateral (*bl.*) 2FLI. CBX did not inhibit effects of basolateral 2FLI. *c,* representative trace of ~50% increase in CBF with apical 2FLI in IL-13–treated ALI (21 days differentiation then 4 subsequent days with IL-13). *d–f,* representative traces showing CBF in the presence of gap junction inhibitors CBX (*d* and *e*) or Gap 27 (*f*; 10 μM; 30 min pretreatment) in cultures treated with IL-13. Apical 2FLI responses were blocked, but basolateral 2 FLI (*d*) or apical ATP (*e* and *f*) responses were intact. *g, bar graph* showing *peak normalized CBF* with agonist as used in *a–f*. Control cultures are shown in *green,* and IL-13 cultures are shown in *magenta*. Each data point is an independent ALI culture from a separate individual patient ($n = 5$ per condition). Significance was determined by one-way ANOVA with Bonferroni post-test; **, $p < 0.01$ between bracketed values. *h* and *i,* schematic of PAR-2 regulation of ciliary function in well-differentiated epithelium (modeled by control cultures; *h*) *versus* remodeled epithelium (modeled by IL-13 stimulated cultures; *i*). Data support that basolateral PAR-2 is expressed under both conditions and can regulate CBF directly within ciliated cells. Apical PAR-2 is not expressed in ciliated cells, but apical PAR-2 stimulation can transmit signals (likely calcium, Ca^{2+}) to ciliated cells through gap junctions. *h* and *i* created with Biorender.com.

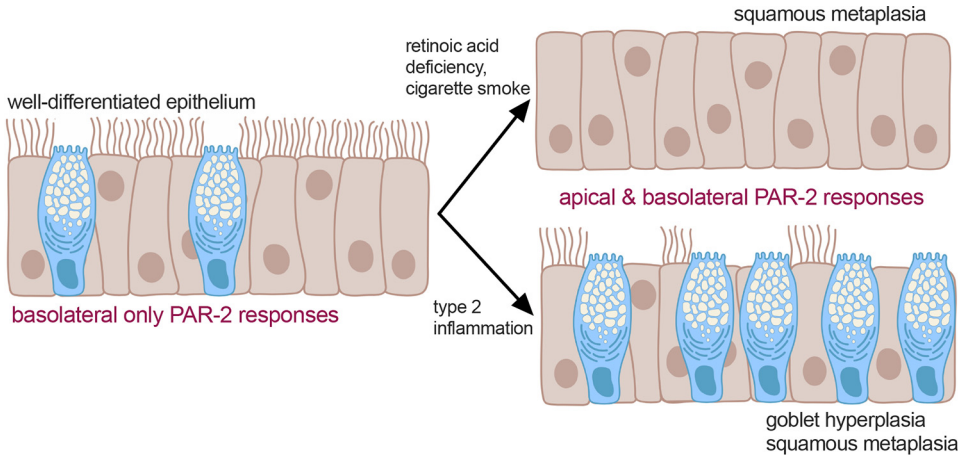

Figure 13. Model of altered PAR-2 signaling in airway disease. We hypothesize that well-differentiated and highly-ciliated airway epithelium can tolerate brief exposure to fungal or dust mite proteases due to the mainly basolateral expression of PAR-2, which is able to activate inflammatory and other responses only if the epithelium is breached. However, airway remodeling through a variety of disease modifiers can change the polarity of epithelial PAR-2 responses and may sensitize the epithelium to proteases *and* thus enhance inflammatory responses. Created with Biorender.com.

glyceraldehyde-3-phosphate dehydrogenase (Hs02786623_g1) in separate reactions, and relative expression was calculated by calculated by means of the $2^{-\Delta\Delta Ct}$ method.

Measurement of FITC-conjugated dextran permeability

FITC-conjugated dextran permeability was measured as described previously (66). Briefly, FITC-dextran (10 kDa) in phenol red-free DMEM was placed on the apical side of the culture, and basolateral solution (also phenol red-free DMEM) was collected from the basolateral side after 30 min of incubation at 37 °C. Samples were read in a Tecan Spark 10M fluorescence plate reader at 485 nm excitation and 525 nm emission. Basolateral media from cells treated with apical media only (not FITC-dextran) were used for background subtraction.

Measurement of airway–surface liquid glucose

Glucose permeability was measured as described previously (67). Briefly, glucose permeability was measured by adding 30 μl of glucose-free, phenol red-free DMEM into the apical compartment of 0.33-cm^2 transwells with normal differentiation media placed on the basolateral side. After 6 h of incubation at 37 °C to allow glucose to equilibrate, 25 μl of apical solution was removed to measure glucose concentration using a colorimetric kit (Cayman Chemical) as indicated by the manufacturer's instructions and as described previously (67).

Measurement of CBF

CBF was measured using the Sisson-Ammons Video Analysis system (68) as described previously (8, 62). Briefly, cultures were imaged on a Leica microscope with 20 × 0.8 NA objective and Basler A602f camera running at 100 frames/s. Experiments were carried out at 28 °C. ALIs were washed into HEPES-buffered HBSS containing 1.8 mM Ca^{2+}.

Measurement of cAMP levels by ELISA

Primary sinonasal ALIs were transferred to basolateral HBSS and stimulated with forskolin in 30 μl of apical HBSS ± 2FLI ± FSLLRY-NH_2 as indicated. After 10 min, cells were lysed and assayed for cAMP using cAMP Biotrak Enzyme Immunoassay (EIA) System (GE Healthcare) according to the manufacturer's instructions normalized to mg/ml protein levels. Because we found that baseline cAMP levels were below the limit of detection of this ELISA, we quantified changes in stimulated cAMP, as reported previously (61).

Imaging of ASL height

Imaging of ASL height was performed as described previously (69, 70). Briefly, cultures were first washed twice with 25 μM DTT (5-min prewash) to remove large clumps of airway mucus, followed by at least 5–7 washes with PBS alone to remove residual DTT. ASL was labeled with Texas Red dextran (10,000 M_r; 1 mg/ml) sonicated in perfluorocarbon (PFC-77) ± 2FLI (0.5 mg/ml) and placed in a humidified, heated, and gassed (5% CO_2) stage-top chamber (Tokai Hit; Tokyo, Japan). The apical side of the cultures was otherwise unmodified; any further drug additions were made basolaterally. Spinning disk confocal images were taken using a ×60 (1.0 NA) water immersion objective with 0.2-μm step size. ASL height was determined, as described previously (69), using 70% of maximum fluorescence threshold to define ASL boundaries. For each culture, three separate fields were analyzed, with the averaged value was treated as a single data point.

Imaging of Ca^{2+} in cells and tissue explants

Calcium imaging was performed as described previously (8, 46, 61, 62). Submerged RMPI 2650 and NCI–H520 cells were loaded with 5 μM Fluo-4 for 45 min, and Ca^{2+} was imaged as described previously (8, 61, 62). Primary human ALIs were loaded, as described previously (8, 46, 61, 62), with 10 μM Fluo-4 acetoxymethyl ester (AM) for 90 min on the apical side. Imaging was performed using a Nikon TS-100 microscope with equipped with 10 × 0.3 NA PlanFluor objective (for ALIs) or 20 × 0.8 NA PlanApo objective (for submerged cells) and standard FITC/GFP filter set. Mouse ALIs were loaded similarly with Calbryte 590 to avoid green autofluorescence and visualized with TRITC filter set. Background was estimated by imaging unloaded ALIs or off cell region for submerged cells at identical settings as described (46). Experiments utilized HBSS buffered with 20 mM HEPES at pH 7.4 with 1.5 mM Ca^{2+} and either 5.5 mM glucose (basolateral side) or 0 glucose (apical side). Experiments performed in the absence of Ca^{2+} (0-Ca^{2+}) utilized cultures loaded with BAPTA-AM (10 μM; 15 min preincubation) and extracellular solutions containing no added Ca^{2+} and 1 mM EGTA.

Flat thin sections of mucosa (≥1 mM thick) were cut from middle turbinate or nasal polyp tissue and mounted in an oblong EasyMount Ussing Chamber insert (Harvard Instruments) to isolate the apical and basolateral surfaces. The tissue and insert were then placed apical side up in a Petri dish containing HBSS containing 1× MEM amino acids, 1× MEM vitamins, 2 mM L-glutamine. The apical side was loaded with 15 μM Calbryte 590-AM in the HBSS solution as above containing 0.4% pluronic F127 for 2 h. Insert was then washed and secured apical side down with vacuum grease on top of a perfusion chamber (Warner Instruments, RC-26GLP) with a low channel and glass coverslip bottom held on a heated stage (Warner PH-1) and perfused with 37 °C Tyrode's buffer, containing (in mM): 140 NaCl, 5 KCl, 2 $CaCl_2$, 1 $MgCl_2$, 10 glucose, 5 Na pyruvate, 10 HEPES, pH 7.4. Imaging was performed on an inverted microscope (Olympus IX83) with a standard TRITC filter set using a 10 × 0.3 NA objective and spinning disk confocal unit (Olympus DSU), XCite 120 LED Boost light source (Excelitas Technologies), Orca Flash 4.0 sCMOS camera (Hamamatsu), and Metafluor using 250-ms exposure and 4 × 4 binning and 5 s sampling frequency to minimize dye bleaching due to the high excitation intensity needed due to the spinning disk.

For measurements of resting $[Ca^{2+}]_i$ in cultures ± CSC, we loaded cultures with 10 μM fura-2-AM in HBSS for 90 min, followed by washing in fura-2–free HBSS. Each culture was imaged for 2 min (one frame every 4 s) to obtain an average baseline fura-2 340/380 emission ratio (R). Cultures were then washed into ionomycin + thapsigargin (10 μg/ml each)-containing HBSS with no added calcium plus 2 mM EGTA on both apical and basolateral sides and imaged after 5 min to obtain R_{min}. Cultures were then washed into buffer containing ionomycin + thapsigargin and 10 mM calcium and imaged after 5

min to obtain R_{max}. Fura-2 340/380 emission ratio was then calibrated to $[Ca^{2+}]_i$ by the method of Grynkiewicz *et al.* (71), as described previously (8, 61, 62).

Data and statistical analysis

Images were acquired in Metamorph, Metafluor, and/or Micromanager (72) and analyzed in FIJI (73). Multiple comparisons were done in GraphPad Prism (La Jolla, CA) using one-way ANOVA with Bonferroni (for pre-selected pairwise comparisons), Tukey-Kramer (for comparing all values), or Dunnett's (for comparing to control value) post-tests; $p < 0.05$ was considered statistically significant. All data are mean ± S.E.

Data availability

All data described are contained within the article and supporting information. Raw numerical data used for generation of graphs are available upon request to the corresponding author (Robert J. Lee, University of Pennsylvania Perelman School of Medicine, E-mail: rjl@pennmedicine.upenn.edu).

Author contributions—R. M. C., J. R. F., B. M. H., N. D. A., J. N. P., and R. J. L. conceptualization; R. M. C., J. R. F., B. M. H., N. D. A., J. N. P., and R. J. L. data curation; R. M. C., J. R. F., B. M. H., N. D. A., and R. J. L. formal analysis; R. M. C. and R. J. L. supervision; R. M. C. and R. J. L. funding acquisition; R. M. C. and R. J. L. validation; R. M. C., J. R. F., B. M. H., N. D. A., and R. J. L. investigation; R. M. C., J. R. F., and R. J. L. writing-original draft; R. M. C., N. D. A., J. N. P., and R. J. L. project administration; R. M. C., J. R. F., B. M. H., N. D. A., J. N. P., and R. J. L. writing-review and editing; N. D. A., J. N. P., and R. J. L. resources.

Acknowledgments—We thank Maureen Victoria (University of Pennsylvania) for technical assistance. We acknowledge Bei Chen (University of Pennsylvania) for isolating and propagating the primary nasal cells used here. We thank Noam Cohen (University of Pennsylvania, Philadelphia Veterans Affairs Medical Center) for access to mouse nasal septum and cigarette smoke condensate and Laura Chandler (Philadelphia Veterans Affairs Medical Center) for fungal cultures.

References

1. Peters, T., and Henry, P. J. (2009) Protease-activated receptors and prostaglandins in inflammatory lung disease. *Br. J. Pharmacol.* **158,** 1017–1033 CrossRef Medline
2. Reed, C. E., and Kita, H. (2004) The role of protease activation of inflammation in allergic respiratory diseases. *J. Allergy Clin. Immunol.* **114,** 997–1008; quiz 1009 CrossRef Medline
3. Molino, M., Barnathan, E. S., Numerof, R., Clark, J., Dreyer, M., Cumashi, A., Hoxie, J. A., Schechter, N., Woolkalis, M., and Brass, L. F. (1997) Interactions of mast cell tryptase with thrombin receptors and PAR-2. *J. Biol. Chem.* **272,** 4043–4049 CrossRef Medline
4. Zhou, J., Perelman, J. M., Kolosov, V. P., and Zhou, X. (2013) Neutrophil elastase induces MUC5AC secretion via protease-activated receptor 2. *Mol. Cell. Biochem.* **377,** 75–85 CrossRef Medline
5. Matsuwaki, Y., Wada, K., White, T., Moriyama, H., and Kita, H. (2012) *Alternaria* fungus induces the production of GM-CSF, interleukin-6, and interleukin-8 and calcium signaling in human airway epithelium through protease-activated receptor 2. *Int. Arch. Allergy Immunol.* **158,** Suppl. 1, 19–29 CrossRef Medline
6. de Boer, J. D., Van't Veer, C., Stroo, I., van der Meer, A. J., de Vos, A. F., van der Zee, J. S., Roelofs, J. J., and van der Poll, T. (2014) Protease-activated receptor-2 deficient mice have reduced house dust mite-evoked allergic lung inflammation. *Innate Immun.* **20,** 618–625 CrossRef Medline
7. Homma, T., Kato, A., Bhushan, B., Norton, J. E., Suh, L. A., Carter, R. G., Gupta, D. S., and Schleimer, R. P. (2016) Role of *Aspergillus fumigatus* in triggering protease-activated receptor-2 in airway epithelial cells and skewing the cells toward a T-helper 2 bias. *Am. J. Respir. Cell Mol. Biol.* **54,** 60–70 CrossRef Medline
8. McMahon, D. B., Workman, A. D., Kohanski, M. A., Carey, R. M., Freund, J. R., Hariri, B. M., Chen, B., Doghramji, L. J., Adappa, N. D., Palmer, J. N., Kennedy, D. W., and Lee, R. J. (2018) Protease-activated receptor 2 activates airway apical membrane chloride permeability and increases ciliary beating. *FASEB J.* **32,** 155–167 CrossRef Medline
9. Yaghi, A., and Dolovich, M. B. (2016) Airway epithelial cell cilia and obstructive lung disease. *Cells* **5,** 40 CrossRef Medline
10. Gohy, S. T., Hupin, C., Fregimilicka, C., Detry, B. R., Bouzin, C., Gaide Chevronay, H., Lecocq, M., Weynand, B., Ladjemi, M. Z., Pierreux, C. E., Birembaut, P., Polette, M., and Pilette, C. (2015) Imprinting of the COPD airway epithelium for dedifferentiation and mesenchymal transition. *Eur. Respir. J.* **45,** 1258–1272 CrossRef Medline
11. Chilvers, M. A., McKean, M., Rutman, A., Myint, B. S., Silverman, M., and O'Callaghan, C. (2001) The effects of coronavirus on human nasal ciliated respiratory epithelium. *Eur. Respir J.* **18,** 965–970 CrossRef Medline
12. Wu, N. H., Yang, W., Beineke, A., Dijkman, R., Matrosovich, M., Baumgärtner, W., Thiel, V., Valentin-Weigand, P., Meng, F., and Herrler, G. (2016) The differentiated airway epithelium infected by influenza viruses maintains the barrier function despite a dramatic loss of ciliated cells. *Sci. Rep.* **6,** 39668 CrossRef Medline
13. Mata, M., Sarrion, I., Armengot, M., Carda, C., Martinez, I., Melero, J. A., and Cortijo, J. (2012) Respiratory syncytial virus inhibits ciliagenesis in differentiated normal human bronchial epithelial cells: effectiveness of *N*-acetylcysteine. *PLoS ONE* **7,** e48037 CrossRef Medline
14. Hao, Y., Kuang, Z., Walling, B. E., Bhatia, S., Sivaguru, M., Chen, Y., Gaskins, H. R., and Lau, G. W. (2012) *Pseudomonas aeruginosa* pyocyanin causes airway goblet cell hyperplasia and metaplasia and mucus hypersecretion by inactivating the transcriptional factor FoxA2. *Cell. Microbiol.* **14,** 401–415 CrossRef Medline
15. Park, K. S., Wells, J. M., Zorn, A. M., Wert, S. E., Laubach, V. E., Fernandez, L. G., and Whitsett, J. A. (2006) Transdifferentiation of ciliated cells during repair of the respiratory epithelium. *Am. J. Respir. Cell Mol. Biol.* **34,** 151–157 CrossRef Medline
16. Sisson, J. H., Papi, A., Beckmann, J. D., Leise, K. L., Wisecarver, J., Brodersen, B. W., Kelling, C. L., Spurzem, J. R., and Rennard, S. I. (1994) Smoke and viral infection cause cilia loss detectable by bronchoalveolar lavage cytology and dynein ELISA. *Am. J. Respir. Crit. Care Med.* **149,** 205–213 CrossRef Medline
17. Tamashiro, E., Xiong, G., Anselmo-Lima, W. T., Kreindler, J. L., Palmer, J. N., and Cohen, N. A. (2009) Cigarette smoke exposure impairs respiratory epithelial ciliogenesis. *Am. J. Rhinol. Allergy* **23,** 117–122 CrossRef Medline
18. Chaaban, M. R., Kejner, A., Rowe, S. M., and Woodworth, B. A. (2013) Cystic fibrosis chronic rhinosinusitis: a comprehensive review. *Am. J. Rhinol. Allergy* **27,** 387–395 CrossRef Medline
19. Mynatt, R. G., Do, J., Janney, C., and Sindwani, R. (2008) Squamous metaplasia and chronic rhinosinusitis: a clinicopathological study. *Am. J. Rhinol.* **22,** 602–605 CrossRef Medline
20. Pawankar, R., and Nonaka, M. (2007) Inflammatory mechanisms and remodeling in chronic rhinosinusitis and nasal polyps. *Curr. Allergy Asthma Rep.* **7,** 202–208 CrossRef Medline
21. Chaudhary, N., and Marr, K. A. (2011) Impact of *Aspergillus fumigatus* in allergic airway diseases. *Clin. Transl. Allergy* **1,** 4 CrossRef Medline
22. Daines, M. O., Flynn, A., Sherwood, C., Shultz, S., Hoffman, J., Gruzinova, I., and Boitano, S. (2011) PAR-2 activation by *Alternaria alternata* proteases induces airway epithelial cell activation and lung inflammation. *J. Allergy Clin. Immunol.* **127,** CrossRef
23. Boitano, S., Flynn, A. N., Sherwood, C. L., Schulz, S. M., Hoffman, J., Gruzinova, I., and Daines, M. O. (2011) *Alternaria alternata* serine proteases induce lung inflammation and airway epithelial cell activation via PAR2. *Am. J. Physiol. Lung Cell Mol. Physiol.* **300,** L605–L614 CrossRef Medline

24. Niu, Y., Zhao, G., Li, C., Lin, J., Jiang, N., Che, C., Zhang, J., and Xu, Q. (2018) *Aspergillus fumigatus* increased PAR-2 expression and elevated proinflammatory cytokines expression through the pathway of PAR-2/ERK1/2 in cornea. *Invest. Ophthalmol. Vis. Sci.* **59,** 166–175 CrossRef Medline
25. Dagenais, T. R., and Keller, N. P. (2009) Pathogenesis of *Aspergillus fumigatus* in invasive aspergillosis. *Clin. Microbiol. Rev.* **22,** 447–465 CrossRef Medline
26. Zhang, Q., Zheng, Y. W., Coughlin, S. R., and Shu, X. (2018) A rapid fluorogenic GPCR–β-arrestin interaction assay. *Protein Sci.* **27,** 874–879 CrossRef Medline
27. Eichel, K., and von Zastrow, M. (2018) Subcellular organization of GPCR signaling. *Trends Pharmacol. Sci.* **39,** 200–208 CrossRef Medline
28. Gieseler, F., Ungefroren, H., Settmacher, U., Hollenberg, M. D., and Kaufmann, R. (2013) Proteinase-activated receptors (PARs)–focus on receptor-receptor-interactions and their physiological and pathophysiological impact. *Cell Commun. Signal.* **11,** 86 CrossRef Medline
29. Zhao, P., Lieu, T., Barlow, N., Sostegni, S., Haerteis, S., Korbmacher, C., Liedtke, W., Jimenez-Vargas, N. N., Vanner, S. J., and Bunnett, N. W. (2015) Neutrophil elastase activates protease-activated receptor-2 (PAR2) and transient receptor potential vanilloid 4 (TRPV4) to cause inflammation and pain. *J. Biol. Chem.* **290,** 13875–13887 CrossRef Medline
30. Ramachandran, R., Mihara, K., Chung, H., Renaux, B., Lau, C. S., Muruve, D. A., DeFea, K. A., Bouvier, M., and Hollenberg, M. D. (2011) Neutrophil elastase acts as a biased agonist for proteinase-activated receptor-2 (PAR2). *J. Biol. Chem.* **286,** 24638–24648 CrossRef Medline
31. Dulon, S., Leduc, D., Cottrell, G. S., D'Alayer, J., Hansen, K. K., Bunnett, N. W., Hollenberg, M. D., Pidard, D., and Chignard, M. (2005) *Pseudomonas aeruginosa* elastase disables proteinase-activated receptor 2 in respiratory epithelial cells. *Am. J. Respir. Cell Mol. Biol.* **32,** 411–419 CrossRef Medline
32. Dulon, S., Candé, C., Bunnett, N. W., Hollenberg, M. D., Chignard, M., and Pidard, D. (2003) Proteinase-activated receptor-2 and human lung epithelial cells: disarming by neutrophil serine proteinases. *Am. J. Respir. Cell Mol. Biol.* **28,** 339–346 CrossRef Medline
33. Lachowicz-Scroggins, M. E., Boushey, H. A., Finkbeiner, W. E., and Widdicombe, J. H. (2010) Interleukin-13–induced mucous metaplasia increases susceptibility of human airway epithelium to rhinovirus infection. *Am. J. Respir. Cell Mol. Biol.* **43,** 652–661 CrossRef Medline
34. Yu, H., Li, Q., Kolosov, V. P., Perelman, J. M., and Zhou, X. (2010) Interleukin-13 induces mucin 5AC production involving STAT6/SPDEF in human airway epithelial cells. *Cell Commun. Adhes.* **17,** 83–92 CrossRef Medline
35. Lopez-Souza, N., Dolganov, G., Dubin, R., Sachs, L. A., Sassina, L., Sporer, H., Yagi, S., Schnurr, D., Boushey, H. A., and Widdicombe, J. H. (2004) Resistance of differentiated human airway epithelium to infection by rhinovirus. *Am. J. Physiol. Lung Cell Mol. Physiol.* **286,** L373–L381 CrossRef Medline
36. Million, K., Tournier, F., Houcine, O., Ancian, P., Reichert, U., and Marano, F. (2001) Effects of retinoic acid receptor-selective agonists on human nasal epithelial cell differentiation. *Am. J. Respir. Cell Mol. Biol.* **25,** 744–750 CrossRef Medline
37. Vollberg, T. M., George, M. D., Nervi, C., and Jetten, A. M. (1992) Regulation of type I and type II transglutaminase in normal human bronchial epithelial and lung carcinoma cells. *Am. J. Respir. Cell Mol. Biol.* **7,** 10–18 CrossRef Medline
38. Yoshida, T., Matsuwaki, Y., Asaka, D., Hama, T., Otori, N., and Moriyama, H. (2013) The expression of protease-activated receptors in chronic rhinosinusitis. *Int. Arch. Allergy Immunol.* **161,** Suppl. 2, 138–146 CrossRef Medline
39. Ramachandran, R., Sadofsky, L. R., Xiao, Y., Botham, A., Cowen, M., Morice, A. H., and Compton, S. J. (2007) Inflammatory mediators modulate thrombin and cathepsin-G signaling in human bronchial fibroblasts by inducing expression of proteinase-activated receptor-4. *Am. J. Physiol. Lung Cell Mol. Physiol* **292,** L788–L798 CrossRef Medline
40. Saito, A., Horie, M., and Nagase, T. (2018) TGF-β signaling in lung health and disease. *Int. J. Mol. Sci.* **19,** 2460 CrossRef Medline
41. Hwang, P. H., and Chan, J. M. (2006) Retinoic acid improves ciliogenesis after surgery of the maxillary sinus in rabbits. *Laryngoscope* **116,** 1080–1085 CrossRef Medline
42. Gray, T. E., Guzman, K., Davis, C. W., Abdullah, L. H., and Nettesheim, P. (1996) Mucociliary differentiation of serially passaged normal human tracheobronchial epithelial cells. *Am. J. Respir. Cell Mol. Biol.* **14,** 104–112 CrossRef Medline
43. Son, H. L., Park, H. R., Park, Y. J., and Kim, S. W. (2015) Effect of retinoic acid in a mouse model of allergic rhinitis. *Allergy Asthma Immunol. Res.* **7,** 590–598 CrossRef Medline
44. Hufnagl, K., and Jensen-Jarolim, E. (2018) Vitamin A and D in allergy: from experimental animal models and cellular studies to human disease. *Allergo J. Int.* **27,** 72–78 CrossRef Medline
45. Kim, S. W., Cheon, K., Kim, C. H., Yoon, J. H., Hawke, D. H., Kobayashi, R., Prudkin, L., Wistuba, I. I., Lotan, R., Hong, W. K., and Koo, J. S. (2007) Proteomics-based identification of proteins secreted in apical surface fluid of squamous metaplastic human tracheobronchial epithelial cells cultured by three-dimensional organotypic air-liquid interface method. *Cancer Res.* **67,** 6565–6573 CrossRef Medline
46. Lee, R. J., Xiong, G., Kofonow, J. M., Chen, B., Lysenko, A., Jiang, P., Abraham, V., Doghramji, L., Adappa, N. D., Palmer, J. N., Kennedy, D. W., Beauchamp, G. K., Doulias, P.-T., Ischiropoulos, H., Kreindler, J. L., *et al.* (2012) T2R38 taste receptor polymorphisms underlie susceptibility to upper respiratory infection. *J. Clin. Invest.* **122,** 4145–4159 CrossRef Medline
47. Rudack, C., Steinhoff, M., Mooren, F., Buddenkotte, J., Becker, K., von Eiff, C., and Sachse, F. (2007) PAR-2 activation regulates IL-8 and GRO-α synthesis by NF-κB, but not RANTES, IL-6, eotaxin or TARC expression in nasal epithelium. *Clin. Exp. Allergy* **37,** 1009–1022 CrossRef Medline
48. Palmer, M. L., Lee, S. Y., Maniak, P. J., Carlson, D., Fahrenkrug, S. C., and O'Grady, S. M. (2006) Protease-activated receptor regulation of Cl- secretion in Calu-3 cells requires prostaglandin release and CFTR activation. *Am. J. Physiol. Cell Physiol.* **290,** C1189–C1198 CrossRef Medline
49. Cho, H. J., Choi, J. Y., Yang, Y. M., Hong, J. H., Kim, C. H., Gee, H. Y., Lee, H. J., Shin, D. M., and Yoon, J. H. (2010) House dust mite extract activates apical Cl(−) channels through protease-activated receptor 2 in human airway epithelia. *J. Cell. Biochem.* **109,** 1254–1263 CrossRef Medline
50. Joo, N. S., Evans, I. A., Cho, H. J., Park, I. H., Engelhardt, J. F., and Wine, J. J. (2015) Proteomic analysis of pure human airway gland mucus reveals a large component of protective proteins. *PLoS ONE* **10,** e0116756 CrossRef Medline
51. Joo, N. S., Lee, D. J., Winges, K. M., Rustagi, A., and Wine, J. J. (2004) Regulation of antiprotease and antimicrobial protein secretion by airway submucosal gland serous cells. *J. Biol. Chem.* **279,** 38854–38860 CrossRef Medline
52. Jenkins, H. A., Cool, C., Szefler, S. J., Covar, R., Brugman, S., Gelfand, E. W., and Spahn, J. D. (2003) Histopathology of severe childhood asthma: a case series. *Chest* **124,** 32–41 CrossRef Medline
53. Cluroe, A., Holloway, L., Thomson, K., Purdie, G., and Beasley, R. (1989) Bronchial gland duct ectasia in fatal bronchial asthma: association with interstitial emphysema. *J. Clin. Pathol.* **42,** 1026–1031 CrossRef Medline
54. Chen, F. H., Samson, K. T., Miura, K., Ueno, K., Odajima, Y., Shougo, T., Yoshitsugu, Y., and Shioda, S. (2004) Airway remodeling: a comparison between fatal and nonfatal asthma. *J. Asthma* **41,** 631–638 CrossRef Medline
55. Jeffery, P. K., and Brain, A. P. (1988) Surface morphology of human airway mucosa: normal, carcinoma or cystic fibrosis. *Scanning Microsc.* **2,** 553–560 Medline
56. Yee, K. K., Pribitkin, E. A., Cowart, B. J., Vainius, A. A., Klock, C. T., Rosen, D., Hahn, C. G., and Rawson, N. E. (2009) Smoking-associated squamous metaplasia in olfactory mucosa of patients with chronic rhinosinusitis. *Toxicol. Pathol.* **37,** 594–598 CrossRef Medline
57. Goncalves, V. S. S., Matias, A. A., Poejo, J., Serra, A. T., and Duarte, C. M. M. (2016) Application of RPMI 2650 as a cell model to evaluate solid formulations for intranasal delivery of drugs. *Int. J. Pharm.* **515,** 1–10 CrossRef Medline
58. Wengst, A., and Reichl, S. (2010) RPMI 2650 epithelial model and three-dimensional reconstructed human nasal mucosa as *in vitro* models for

nasal permeation studies. *Eur. J. Pharm. Biopharm.* **74,** 290–297 CrossRef Medline

59. Salib, R. J., Lau, L. C., and Howarth, P. H. (2005) The novel use of the human nasal epithelial cell line RPMI 2650 as an *in vitro* model to study the influence of allergens and cytokines on transforming growth factor-β gene expression and protein release. *Clin. Exp. Allergy* **35,** 811–819 CrossRef Medline
60. Lewandowska-Polak, A., Brauncajs, M., Paradowska, E., Jarzebska, M., Kurowski, M., Moskwa, S., Lesnikowski, Z. J., and Kowalski, M. L. (2015) Human parainfluenza virus type 3 (HPIV3) induces production of IF-Ngamma and RANTES in human nasal epithelial cells (HNECs). *J. Inflamm.* **12,** 16 CrossRef Medline
61. Freund, J. R., Mansfield, C. J., Doghramji, L. J., Adappa, N. D., Palmer, J. N., Kennedy, D. W., Reed, D. R., Jiang, P., and Lee, R. J. (2018) Activation of airway epithelial bitter taste receptors by *Pseudomonas aeruginosa* quinolones modulates calcium, cyclic-AMP, and nitric oxide signaling. *J. Biol. Chem.* **293,** 9824–9840 CrossRef Medline
62. Hariri, B. M., McMahon, D. B., Chen, B., Freund, J. R., Mansfield, C. J., Doghramji, L. J., Adappa, N. D., Palmer, J. N., Kennedy, D. W., Reed, D. R., Jiang, P., and Lee, R. J. (2017) Flavones modulate respiratory epithelial innate immunity: anti-inflammatory effects and activation of the T2R14 receptor. *J. Biol. Chem.* **292,** 8484–8497 CrossRef Medline
63. Lee, R. J., Workman, A. D., Carey, R. M., Chen, B., Rosen, P. L., Doghramji, L., Adappa, N. D., Palmer, J. N., Kennedy, D. W., and Cohen, N. A. (2016) Fungal aflatoxins reduce respiratory mucosal ciliary function. *Sci. Rep.* **6,** 33221 CrossRef Medline
64. Mehta, S., Zhang, Y., Roth, R. H., Zhang, J. F., Mo, A., Tenner, B., Huganir, R. L., and Zhang, J. (2018) Single-fluorophore biosensors for sensitive and multiplexed detection of signalling activities. *Nat. Cell Biol.* **20,** 1215–1225 CrossRef Medline
65. Lee, R. J., Hariri, B. M., McMahon, D. B., Chen, B., Doghramji, L., Adappa, N. D., Palmer, J. N., Kennedy, D. W., Jiang, P., Margolskee, R. F., and Cohen, N. A. (2017) Bacterial D-amino acids suppress sinonasal innate immunity through sweet taste receptors in solitary chemosensory cells. *Sci. Signal.* **10,** CrossRef
66. Pothoven, K. L., Norton, J. E., Hulse, K. E., Suh, L. A., Carter, R. G., Rocci, E., Harris, K. E., Shintani-Smith, S., Conley, D. B., Chandra, R. K., Liu, M. C., Kato, A., Gonsalves, N., Grammer, L. C., 3rd., Peters, A. T., *et al.* (2015) Oncostatin M promotes mucosal epithelial barrier dysfunction, and its expression is increased in patients with eosinophilic mucosal disease. *J. Allergy Clin. Immunol.* **136,** 737–746.e4 CrossRef Medline
67. Lee, R. J., Kofonow, J. M., Rosen, P. L., Siebert, A. P., Chen, B., Doghramji, L., Xiong, G., Adappa, N. D., Palmer, J. N., Kennedy, D. W., Kreindler, J. L., Margolskee, R. F., and Cohen, N. A. (2014) Bitter and sweet taste receptors regulate human upper respiratory innate immunity. *J. Clin. Invest.* **124,** 1393–1405 CrossRef Medline
68. Sisson, J. H., Stoner, J. A., Ammons, B. A., and Wyatt, T. A. (2003) All-digital image capture and whole-field analysis of ciliary beat frequency. *J. Microsc.* **211,** 103–111 CrossRef Medline
69. Lee, R. J., Chen, B., Doghramji, L., Adappa, N. D., Palmer, J. N., Kennedy, D. W., and Cohen, N. A. (2013) Vasoactive intestinal peptide regulates sinonasal mucociliary clearance and synergizes with histamine in stimulating sinonasal fluid secretion. *FASEB J.* **27,** 5094–5103 CrossRef Medline
70. McMahon, D. B., Carey, R. M., Kohanski, M. A., Tong, C. C. L., Papagiannopoulos, P., Adappa, N. D., Palmer, J. N., and Lee, R. J. (2020) Neuropeptide regulation of secretion and inflammation in human airway gland serous cells. *Eur. Respir. J.* **2020,** 1901386 CrossRef Medline
71. Grynkiewicz, G., Poenie, M., and Tsien, R. Y. (1985) A new generation of Ca^{2+} indicators with greatly improved fluorescence properties. *J. Biol. Chem.* **260,** 3440–3450 Medline
72. Edelstein, A., Amodaj, N., Hoover, K., Vale, R., and Stuurman, N. (2010) Computer control of microscopes using microManager. *Curr. Protoc. Mol. Biol.* Chapter 14, Unit 14.20 CrossRef Medline
73. Schindelin, J., Arganda-Carreras, I., Frise, E., Kaynig, V., Longair, M., Pietzsch, T., Preibisch, S., Rueden, C., Saalfeld, S., Schmid, B., Tinevez, J. Y., White, D. J., Hartenstein, V., Eliceiri, K., Tomancak, P., and Cardona, A. (2012) Fiji: an open-source platform for biological-image analysis. *Nat. Methods* **9,** 676–682 CrossRef Medline
74. Walker, J. K., and DeFea, K. A. (2014) Role for β-arrestin in mediating paradoxical β2AR and PAR2 signaling in asthma. *Curr. Opin. Pharmacol.* **16,** 142–147 CrossRef Medline
75. Ramachandran, R., Mihara, K., Mathur, M., Rochdi, M. D., Bouvier, M., Defea, K., and Hollenberg, M. D. (2009) Agonist-biased signaling via proteinase activated receptor-2: differential activation of calcium and mitogen-activated protein kinase pathways. *Mol. Pharmacol.* **76,** 791–801 CrossRef Medline
76. Zhao, P., Lieu, T., Barlow, N., Metcalf, M., Veldhuis, N. A., Jensen, D. D., Kocan, M., Sostegni, S., Haerteis, S., Baraznenok, V., Henderson, I., Lindström, E., Guerrero-Alba, R., Valdez-Morales, E. E., Liedtke, W., *et al.* (2014) Cathepsin S causes inflammatory pain via biased agonism of PAR2 and TRPV4. *J. Biol. Chem.* **289,** 27215–27234 CrossRef Medline
77. Jung, S. R., Seo, J. B., Deng, Y., Asbury, C. L., Hille, B., and Koh, D. S. (2016) Contributions of protein kinases and β-arrestin to termination of protease-activated receptor 2 signaling. *J. Gen. Physiol.* **147,** 255–271 CrossRef Medline
78. Cottrell, G. S., Amadesi, S., Schmidlin, F., and Bunnett, N. (2003) Protease-activated receptor 2: activation, signalling and function. *Biochem. Soc. Trans.* **31,** 1191–1197 CrossRef Medline